AD-A099 681 ARCTIC INST OF NORTH AMERICA ARLINGTON VA F/G 8/10
INTERACTIONS WITHIN THE OCEAN-ICE-ATMOSPHERE SYSTEMS OF THE NOR--ETC(U)
FEB 81 J E WALSH, J E SATER N00014-75-C-0635
UNCLASSIFIED NL

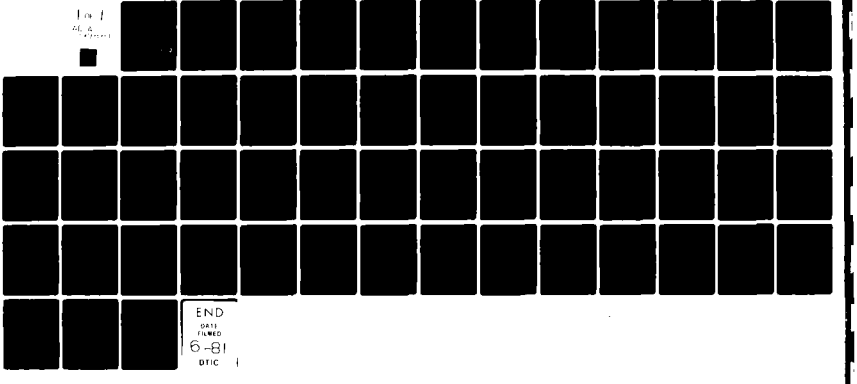

END
DATE FILMED
6-81
DTIC

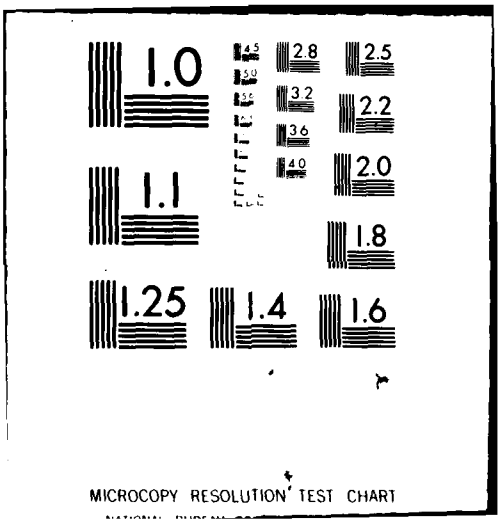
1.0
1.1
1.25
1.4
1.6
1.8
2.0
2.2
2.5
2.8
3.2
3.6
4.0
MICROCOPY RESOLUTION TEST CHART

AD A099681

LEVEL II

Interactions within the ocean-ice-atmosphere systems of the North Pacific and the North Atlantic

John E. Walsh

Laboratory for Atmospheric Research
University of Illinois
Urbana, IL 61801

and

John E. Sater

Arctic Institute of North America
Arlington, VA 22201

DTIC ELECTE JUN 3 1981 S D A

N00014-75C-0635

This document has been approved for public release and sale; its distribution is unlimited.

September 1980

(Revised Feb 81)

DTIC FILE COPY

033 050

81 6 03 042

ABSTRACT

Four regional indices of sea ice variability and thirty years of monthly sea surface temperature (SST) and sea level pressure (SLP) data are used to evaluate the large-scale interactions within the ocean-ice-atmosphere systems of the North Pacific and the North Atlantic. A direct association between positive (negative) SST anomalies and light (heavy) ice in the Bering Sea is indicated. The SST/ice coupling in the northern Alaskan waters is also statistically significant. The SST anomalies in both the North Pacific and the North Atlantic appear as persistent responses to atmospheric forcing. The SLP distributions over both oceans correlate significantly with the arctic SLP distribution, although the midlatitude atmospheric circulation shows no systematic tendency to lead or lag the arctic circulation. Sea ice fluctuations correlate most highly with the atmospheric forcing over antecedent periods of approximately 9 months in the northern Alaskan waters, 3-4 months in the Bering Sea, and 5-7 months in the East Greenland Sea. The strength of the 9-month mean onshore air flow component describes over 70% of the northern Alaskan ice variance.

Accession For
GRA&I
TAB
Unannounced
Justification
Distribution/
Availability Codes
Avail and/or
Special
A

A

1. INTRODUCTION

A sizable literature on the subject of large-scale interactions between sea ice and the atmosphere has evolved in recent years. The existence of coherent fluctuations of ice extent over thousands of kilometers has been identified by Walsh and Johnson (1979a), Lemke et al. (1980) and Smirnov (1980). Associations between interannual ice variability and fluctuations in meteorological fields (e.g., sea level pressure, surface temperature, 700 mb height) have been evaluated in varying degrees of detail by Lamb and Mörth (1978), Zakharov and Strokina (1978), Rogers (1978), Rogers and van Loon (1979) and Walsh and Johnson (1979b). While modeling experiments have shown statistically significant atmospheric responses to prescribed extremes of sea ice extent (Herman and Johnson, 1979), the consensus emerging from the data-based studies is that large-scale ice anomalies correlate more highly with antecedent than with subsequent meteorological fluctuations. The percentage of ice variability that may be specified in a hindcast sense from meteorological data appears to be on the order of 10-70% depending on the region, the temporal resolution, the quality of the ice data and the choice of the meteorological variables.

Commonly cited sources of the "unexplained" ice variance are oceanic factors such as variable ocean currents and sea surface temperature (SST) distributions (e.g., Haupt and Kant, 1976). Schell (1970) and Rogers and van Loon (1979) have demonstrated the compatibility of large-scale SST and sea ice variations in selected regions and selected years. Considerably more effort has been expended recently in the evaluation of the coupling between large-scale SST and atmospheric circulation anomalies over the North Pacific (e.g., Namias, 1976; Davis, 1978; Elsberry and Raney, 1978; Broccoli and Harnack, 1981) and the North Atlantic (e.g., Ratcliffe, 1973; Rowntree,

1976; Haworth, 1978). Since the results of these studies have indicated the existence of statistically significant associations between SST anomalies and the atmospheric circulation, the link between SST fields and the high-latitude sea ice distribution must be viewed in the context of Figure 1. The "direct association", in which high SSTs enhance melting and retard freezing, is to be distinguished from the "indirect association", in which the sea ice distribution is influenced by SST through an SST-induced effect on the atmospheric circulation. The evaluation of the SST-ice coupling from observational data is complicated by the possibility that both coupling mechanisms may act simultaneously.

The present work is an attempt to identify the associations between the SST distribution, the atmospheric circulation and the interannual variability of sea ice in several regions within the marginal ice zone: the northern Alaskan waters from Cape Prince of Wales to Demarcation Point (summer), the Bering Sea (winter), the East Greenland Sea (summer) and the Denmark Strait (winter). Alternatively, by using the distribution of sea level pressure (SLP) to represent the low-level atmospheric circulation, we wish to evaluate the relative strengths and directions of the three links represented in Figure 1: SST/ice, SST/SLP and SLP/ice. Such an evaluation can have direct implications about causal mechanisms in the three-component system. For example, a cross-correlation function that is asymmetric about 0 lag can aid in the establishment of cause and effect. Cross-correlation functions will therefore be evaluated in an attempt to answer the following questions:

(i) Are high-latitude SST fluctuations generally causes or effects of large-scale sea ice fluctuations?

(ii) Are middle- and high-latitude SST fluctuations generally causes or effects of atmospheric circulation anomalies?

(iii) How does the link between SST and sea ice compare quantitatively to the link between SLP and sea ice?

Within the context of the three-component analysis, several additional items will be addressed. Among these are the seasonality inherent in (i)-(iii), differences between the air-sea-ice systems of the North Atlantic and the North Pacific, and the time scales that are pertinent to the evolution of large-scale ice anomalies. The latter item will have direct implications for the predictability of large-scale sea ice fluctuations. Finally, the examination of the indirect association of Figure 1 will require the evaluation of "teleconnections" or lead/lag relationships between the arctic and midlatitude atmospheric circulations. While the existence of significant lead/lag relationships of this type would assign directionality to arctic/midlatitude interactions, the subject of arctic/midlatitude teleconnections has received surprisingly little attention since Namias' (1958) analysis of several examples of arctic circulation anomalies.

The data analysis is based on monthly grids of SLP, SST and sea ice extent. The use of the monthly time unit places some constraints on the inferences concerning the time scales of the system. However, the available data on SST and sea ice preclude more detailed temporal resolution. Spatial variability will be incorporated into the analysis through the use of the dominant *patterns* of SST and SLP variability. Pattern analysis is used because SST and SLP fields are characterized by large amounts of spatial coherence (e.g., Namias and Born, 1970; Davis, 1976). Considerable redundancy would therefore result from the use of individual grid point values.

Section 2 describes the sources, resolution and some limitations of the data. The distributions and patterns that form the basis of the correlative analysis are presented in Section 3, while the results and implications of the correlative analysis are discussed in Section 4.

2. DATA

The study is based on monthly SLP and SST data grids for the years 1948-1977 and on monthly sea ice grids for the years 1953-1977. A total of 300 grids of sea ice and 360 grids each of SLP and SST are therefore used in the analysis.

The sea level pressure data, which are in the form of 5°x5° latitude-longitude grids from 20°N-90°N, were obtained from the National Center for Atmospheric Research (NCAR). While the NCAR grids are based on several sources (Jenne, 1975), the primary source during the 1948-1977 period was the U.S. Navy Fleet Numerical Weather Center. The use of the high-latitude portions of these grids introduces the risk of data unreliability (e.g., Albright, 1980). Trenberth and Paolino (1980) have found that discontinuities associated with erroneously high arctic pressures appeared primarily in the 1920's, after which time there was little evidence of such errors. In addition, tabulations of arctic drift station data were used in the present study to check the accuracy of the NCAR analyses in the Arctic. The discrepancies between the observed (monthly) station pressures and the analyzed values were generally less than 2 mb. The errors are therefore considerably smaller than the typical standard deviations (3-6 mb) of the high-latitude pressures.

The sea ice grids are the monthly ice concentration grids described by Walsh and Johnson (1979a). These grids contain the fractions (tenths) of

ice coverage regardless of ice type and thickness in a set of grid squares 60 n mi (111 km) on a side. As discussed in Section 3, the ice variables used in the present work are departures from the 25-year monthly mean areal coverage of ice in several longitudinal sectors of 30°-40° each. Each such departure was obtained by a summation of the products of the ice concentrations and corresponding ocean areas in all grid squares of the longitudinal sector.

The sea surface temperature grids were obtained from several sources. The North Pacific data are in the form of monthly 5°x5° latitude-longitude grids covering the ocean areas from 20°N-60°N and 130°E-110°W. These grids were compiled at the Scripps Institute of Oceanography and were supplied to us by R. Born and J. Namias. While the Scripps data set covers the period from January, 1947 through the present, only the grids for 1948-1977 are used here. North Atlantic grids for the years 1948-1967 were obtained from a "quality-controlled" version of the Tape Data Family 11 (TDF11) which was compiled from several sources by the National Weather Records Center, Asheville, NC. These grids cover the ocean areas of the northern hemisphere between 0° and 80°N with a resolution of 5°x5°. The quality control process, in which large values of normalized monthly departures were discarded, was carried out at the British Meteorological Office in Bracknell, England. A copy of the "polished" data set was obtained from NCAR. North Atlantic SST data for the years 1963-1977 were obtained from the hemispheric surface temperature analyses of the U.S. Navy. These analyses were interpolated bilinearly from the Navy's 63x63 polar stereographic grid onto the latitude-longitude grid of the TDF11 data set. The North Atlantic grids from each source were then converted to departures from the monthly mean SSTs derived from that source only. The subtraction of monthly means

computed from the individual data sets served to minimize the effect of any discontinuities introduced by the consolidation of the two data sets. Correlations between the two sets of monthly anomalies were computed for the five years (1963-1967) of data overlap; these correlations ranged from 0.70 to 0.92 over a set of 50 grid points in different portions of the North Atlantic. The common variance between the two data sets therefore ranged from 0.49 to 0.83. Since the discrepancies represent substantial portions of the SST variance, the results of a correlative analysis based on the North Atlantic SST data must be regarded as lower bounds on the coupling between the SST fields and the other variables. As a compromise between the uncertainties in the two data sets, algebraic means of the monthly anomalies from the two sources were used for the 1963-1967 period.

It should be noted that the Scripps and TDF11 data sets often do not include data values within 5° latitude of the ice edge. While these missing values are attributable to the scarcity of observations near the ice edge, they limit the evaluation of the "direct" association between SST and ice extent. The analyses in the following two sections are based on 50 North Pacific and 50 North Atlantic grid points that were chosen for spatial uniformity subject to the constraint that no single point be missing from more than 15% of the total number of grids.

3. DATA REPRESENTATIONS

a. Sea ice

The areal coverage of sea ice was evaluated for Atlantic and Pacific sectors of 30-40° longitude for three-month periods centered on the approximate months (March and August) of minimum and maximum ice extent. The longitudinal sectors will be referred to as the northern Alaskan waters

(NA, 140°W-170°W), the Bering Sea (BS, 150°W-180°W), the East Greenland Sea (EG, 20°W-20°E) and the Denmark Strait northwest of Iceland (DS, 10°W-40°W). Ice extent is presented as sums of departures from the normal areal coverage for July-September in the northern Alaskan and East Greenland regions, and as the corresponding sums for February-April in the Bering Sea and the Denmark Strait. The analysis therefore addresses wintertime ice variability in two southern regions and summertime ice variability in two northern regions within the seasonal sea ice zone. Figure 2 shows the 25-year time series of ice coverage in each of the four regions. Considerable interannual variability is apparent in every region, although the two plots for the winter season (I_{BS} and I_{DS}) show a greater tendency for the clustering of heavy and light ice years. Ice extent in the Bering Sea was generally below the 25-year mean during the 1960's and above the mean during the 1970's, while ice in the Denmark Strait was generally below normal during the first half of the period and above normal during the 1965-1970 period. However, none of the 25-year trends were found to be statistically significant. The increase in Bering sea ice during the early and middle 1970's was also reported by Niebauer (1980). The time series for the northern Alaskan ice correlates at -0.895 with Barnett's (1980) Alaskan ice severity index, which ranges from 0 for the most severe shipping season (1975) to 624 for the most favorable shipping season (1958) of the 25-year period.

Table 1 contains the correlations between the four regional indices of ice coverage. The 0-lag correlations, which are based on pairs of values from the same calendar year, were found to be positive for regions in the same hemisphere (Atlantic or Pacific) and negative for regions in opposite hemispheres. Since the 95% significance level for a sample of 25 (independent) pairs of values is 0.40, the EG/DS correlation of 0.57 indicates a

statistically significant tendency for winter anomalies in the Denmark Strait to be followed by summer anomalies of the same sign in the East Greenland Sea. The negative values of the Atlantic vs. Pacific correlations (EG vs. NA, EG vs. BS, DS vs. BS) provide modest quantitative support for Smirnov's (1980) contention that ice anomalies in the eastern and western Arctic are generally of opposite sign. These negative correlations are also consistent with recently computed sets of sea ice eigenvectors (Lemke et al., 1980; Walsh and Johnson, 1979b) which indicate that the most common modes of large-scale ice variability contain positive anomalies in some longitudes and negative anomalies in others. The lag 0 correlations between the Atlantic and Pacific indices are, however, only marginally significant at the 95% level.

The lag 1 correlations of Table 1 show the tendency for departures in the Bering Sea and the Denmark Strait to be of the same sign as the departures during the previous summer in the same hemisphere. In addition, the year-to-year persistences (0.50 and 0.52) of the two wintertime series contrast with the negligible persistences (0.03 and -0.07) of the summer series. The relatively large persistences of the wintertime indices are statistical measures of the tendency for the clustering of heavy and light ice years in the two wintertime series (I_{BS} and I_{DS}) of Figure 2.

b. Sea level pressure and sea surface temperature

In view of the large volume of SLP and SST data, much of the analysis and discussion is based on the dominant *patterns* of variability of the data fields. These patterns are empirical orthogonal functions (EOFs), which are also referred to as eigenvectors or principal components. The first eigenvector of a set of data fields is the dominant mode of variability in the sense that it describes a greater percentage of the variance of the data

fields than does any other pattern. Each succeeding eigenvector describes a maximum of the variance that is unexplained by the previous eigenvectors. The coefficient or amplitude of an eigenvector is a measure of the extent to which that eigenvector pattern is present in a particular anomaly field. The various time series of the eigenvector coefficients form the basis of the statistical analysis in Section 4. Among the advantages of the eigenvector representation are the effective compression of the data and the orthogonality (independence) of the patterns in space and time.

Since a goal of the analysis was the evaluation of the directions and relative strengths of the links in Figure 1, sets of eigenvectors were computed for SST in the midlatitude ocean and SLP in middle and high latitudes. These three sets of patterns were computed separately for the North Pacific sector and for the North Atlantic sector. All eigenvectors were computed using normalized departures from monthly means. The normalization involved a subtraction of the monthly mean (SLP or SST) for the grid point and a division by the standard deviation for that grid point and calendar month. This procedure removes the seasonal cycle that otherwise would concentrate most of the variance into a single mode (e.g., Weare, 1977) and avoids an overweighting of high-variance regions in the resulting patterns. Because the spatial domain of each set of eigenvectors in the present study is relatively limited, the spatial bias introduced into the eigenvectors by the normalization is less problematic than in studies of hemispheric patterns (e.g., Rogers, 1979).

(1) Pacific patterns

Figures 3 and 4 show the first four eigenvectors of the Pacific SLP sets, $\underset{\sim}{P}^{MP}$ (Midlatitude Pacific) and $\underset{\sim}{P}^{HP}$ (High-latitude Pacific).[1] Each set was computed from a network of 50 grid points represented by dots in the figures. Table 2 summarizes the major features of the various sets of eigenvectors. Both $\underset{\sim}{P}_1^{MP}$ and $\underset{\sim}{P}_2^{MP}$ contain north-south gradients from which anomalous east-west geostrophic airflow may be inferred. The strongest pressure gradient is approximately 5-10° farther southward in $\underset{\sim}{P}_2^{MP}$ than in $\underset{\sim}{P}_1^{MP}$. The results in Section 4a will support the hypothesis that $\underset{\sim}{P}_1^{MP}$ and $\underset{\sim}{P}_2^{MP}$ are summer and winter manifestations of the same pattern, which corresponds to a mass exchange between the Aleutian low and the Pacific subtropical high. Southward shifts of 5-10° from summer to winter are typical of these semi-permanent features. $\underset{\sim}{P}_3^{MP}$ and $\underset{\sim}{P}_4^{MP}$ represent somewhat more complex anomalies, although the implicit north-south airflow over the Bering Sea is pertinent to the interpretation of the correlative results in Section 4. The patterns $\underset{\sim}{P}_1^{MP}$ - $\underset{\sim}{P}_4^{MP}$ describe 65.4% of the variance contained in the entire set of 50 midlatitude Pacific pressure eigenvectors.

The first four high-latitude Pacific pressure patterns, $\underset{\sim}{P}_1^{HP}$ - $\underset{\sim}{P}_4^{HP}$, are shown in Figure 4 and summarized in Table 2. These four patterns describe 78.6% of the 50-point variance. While $\underset{\sim}{P}_1^{HP}$ represents a general excess or deficit of mass with little gradient over the entire domain, $\underset{\sim}{P}_2^{HP}$ and $\underset{\sim}{P}_3^{HP}$ describe large gradients in approximately perpendicular directions. The corresponding geostrophic airflow and ice drift are north-south in $\underset{\sim}{P}_2^{HP}$ and

[1] In the sections that follow, vector notation ($\underset{\sim}{P}^{MP}$, $\underset{\sim}{T}^{P}$, etc.) is used to denote eigenvectors. The corresponding scalar symbols (P^{MP}, T^{P}, etc.) denote time-dependent amplitudes.

east-west in $\underset{\sim}{P}_3^{HP}$. The importance of $\underset{\sim}{P}_2^{HP}$ in the evolution of Alaskan ice anomalies will become apparent in Section 4.

Comparisons can be made between the patterns of Figures 3-4 and Rogers' (1979) hemispheric eigenvectors, although the latter were computed for the winter season only. $\underset{\sim}{P}_2^{MP}$ appears to correspond with Rogers' second unnormalized eigenvector, which in turn resembled the so-called "North Pacific Oscillation" in pressure. On the other hand, the pattern of zonal flow in $\underset{\sim}{P}_3^{HP}$ is quite similar to the high-latitude circulation in Rogers' first unnormalized eigenvector, which showed a strong resemblance to the "North Atlantic Oscillation" or "Seesaw" (Rogers and van Loon, 1979). Further comparisons are prevented by the limited spatial domain used in the present work and by the restriction of the Rogers and van Loon analysis to the winter season.

The first four patterns of North Pacific sea surface temperature are shown in Figure 5 (see also Table 2). Since these patterns describe only 48% of the 50-eigenvector SST variance, we may infer that the SST fields contain more small-scale variability than do the North Pacific SLP fields. Positive amplitudes of $\underset{\sim}{T}_1^P$, $\underset{\sim}{T}_2^P$ and $\underset{\sim}{T}_3^P$ correspond to negative temperature anomalies in the Aleutian region, although rather large positive anomalies are found south of 45°N. The upper-air anomaly deduced from positive $\underset{\sim}{T}_1^P$ and the thermal wind relationship is an enhanced ridge over the central North Pacific with an anomalous southward component of geostrophic airflow over the eastern North Pacific. (Such reasoning is based on the assumption that the SST anomalies are representative of the temperature gradients in the lower troposphere [Harnack and Broccoli, 1979]). Similarly, positive $\underset{\sim}{T}_2^P$ implies enhanced zonal flow at upper levels above the 30°-40°N latitude belt. The relatively strong anomaly center in $\underset{\sim}{T}_1^P$ at 35°N, 160°W is very

close to the center (40°N, 170°W) of the correlation maps used by Namias (1972) in his analysis of the spatial scales of North Pacific SST anomalies. $\underset{\sim}{T}_1^P$ is also very similar to Davis' (1976) first eigenvector of North Pacific SST.

(2) Atlantic patterns

Figure 6 shows the first four patterns, $\underset{\sim}{P}_1^{MA}$ - $\underset{\sim}{P}_4^{MA}$, of North Atlantic sea level pressure. $\underset{\sim}{P}_1^{MA}$ and $\underset{\sim}{P}_2^{MA}$ correspond very closely to the first two North Pacific patterns. Variations in the intensity of the midlatitude zonal flow are described in each case. The third North Atlantic pattern, which is very similar to $\underset{\sim}{P}_4^{MP}$, represents enhanced northward flow in the North Atlantic waters east of Greenland. The first four North Atlantic patterns describe 60.2% of the 50-eigenvector SLP variance.

The first four patterns of high-latitude North Atlantic pressure, $\underset{\sim}{P}_1^{HA}$ - $\underset{\sim}{P}_4^{HA}$, are shown in Figure 7 and summarized in Table 2. A close correspondence with the Pacific set is again found in the very weak gradient of $\underset{\sim}{P}_1^{HA}$ and the north-south and east-west gradients of $\underset{\sim}{P}_2^{HA}$ and $\underset{\sim}{P}_3^{HA}$. Although the double lobe of high pressure in the southern portion of $\underset{\sim}{P}_3^{HA}$ is somewhat different from the single lobe in $\underset{\sim}{P}_3^{HP}$, the fourth eigenvectors of the two sets are extremely similar. The first four high-latitude North Atlantic patterns describe 76.9% of the 50-eigenvector variance. The patterns $\underset{\sim}{P}_1^{HA}$ and $\underset{\sim}{P}_1^{MA}$ are both quite consistent with Rogers' (1979) first hemispheric eigenvector and with the March sea level pressure difference fields associated with the North Atlantic Oscillation or Seesaw (Rogers and van Loon, 1979, Figure 6). This similarity is detectable even though the eigenvector sets $\underset{\sim}{P}^{MA}$ and $\underset{\sim}{P}^{HA}$ are computed from data for all calendar months.

Figure 8 contains the first four patterns ($\underset{\sim}{T}_1^A$ - $\underset{\sim}{T}_4^A$) of North Atlantic sea surface temperature. $\underset{\sim}{T}_1^A$ resembles the first Pacific SST pattern with a

large anomaly in the central portion of the grid and weaker anomalies of the opposite sign in the northeast and southwest corners. If $\underset{\sim}{T}_1^A$ is representative of temperature anomalies in the lower troposphere, then the thermal wind constraint implies enhanced ridging above the lower troposphere over the North Atlantic. $\underset{\sim}{T}_2^A$, which describes anomalies of a single sign over all but the west-central portion of the grid, shows some resemblance to $\underset{\sim}{T}_3^P$. The generally north-south gradient in $\underset{\sim}{T}_3^A$, on the other hand, is similar to that found in $\underset{\sim}{T}_2^P$. $\underset{\sim}{T}_4^A$ contains some of the finer structure that is typical of the higher modes. The percentage of SST variance described by $\underset{\sim}{T}_1^A - \underset{\sim}{T}_4^A$ is essentially the same as the 48% described by the first four North Pacific SST patterns. These four patterns correspond quite well with the high-latitude portions of Weare's (1977) first four Atlantic SST patterns if the order of $\underset{\sim}{T}_3^A$ and $\underset{\sim}{T}_4^A$ is reversed. However, the agreement between $\underset{\sim}{T}_2^A$ and Weare's second eigenvector is somewhat weak in the eastern North Atlantic.

4. CORRELATIVE ANALYSIS

The results of the analysis will be described separately for the North Pacific (Section 4a) and the North Atlantic (Section 4b). Pertinent similarities and differences between the two regions will be noted.

a. North Pacific

Cross-correlations between the amplitudes of the dominant patterns of SST and middle- and high-latitude SLP were computed in order to assess the teleconnections in the regional ocean-atmosphere system. The 360 monthly grids (1948-1977) of each variable were used in the computations. The correlations are based on 3-month means of the pattern amplitudes in order

to remove some of the high-frequency atmospheric noise. (While the magnitudes of the cross-correlations were found to increase when the averaging period was made longer than 3 months, this increase was at the expense of temporal resolution). A two-dimensional format is used in Figure 9 to show the dependence of several of the correlations on season (calendar month) and on lag, which ranges from -6 to +6 months for each variable. Stippling is used to identify those portions of the lag/season domain where the magnitudes of the correlations exceed 0.4. The 95% and 99% significance levels for a sample size of 30 (years) are 0.36 and 0.48.

The correlations $\langle P^{MP}T^{P}\rangle$ between North Pacific sea level pressure and sea-surface temperature are quite large for several pattern pairs. $\langle P_2^{MP}T_1^{P}\rangle$ exceeds 0.8 during the winter, while the magnitudes of several other correlations exceed 0.7 in certain portions of the year. Several features of the $\langle P^{MP}T^{P}\rangle$ diagrams have important implications concerning the nature of the air/sea coupling. The first such feature is the asymmetry about 0 lag in the distribution of high correlations. Since a large majority of the correlations exceeding 0.4 are found at positive lags of sea surface temperature, the coupling is evidently one in which the atmosphere tends to drive the ocean. Davis (1976) has found a similar directionality in his North Pacific analysis. A second noteworthy feature of the $\langle P^{MP}T^{P}\rangle$ diagrams is the pronounced tendency for the shaded regions to tilt downward and to the right. This tendency suggests that the directionality noted above is due primarily to the persistence of SST anomalies after an oceanic response to atmospheric (SLP) forcing. Elsberry and Raney (1978) have shown that SST anomalies at individual points (Ocean Weather Ships) are attributable largely to limited periods of strong atmospheric forcing (e.g., storms). The

downward/rightward tilt of the larger correlations in the $<P^{MP}T^{P}>$ diagrams of Figure 9 may be manifestations of the effects of this type of atmospheric forcing on a larger spatial scale and on the seasonal time scale. Such interpretations must be considered speculative, however, until supported by more detailed analyses of the evolution of SST anomaly fields.

The signs of the $<P^{MP}T^{P}>$ correlations are generally consistent with reasoning based on advection of SSTs by SLP-induced current anomalies. For example, $<P_1^{MP}T_1^{P}>$, $<P_1^{MP}T_3^{P}>$ and $<P_1^{MP}T_4^{P}>$ represent cases where negative (positive) SST anomalies are found in regions of anomalous southward (northward) or westward (eastward) transport from normally colder (warmer) waters. The interpretation of the large positive $<P_2^{MP}T_1^{P}>$ is less straightforward. Since the coupling between P_2^{MP} and T_1^{P} is clearly a wintertime phenomenon, the earlier interpretation of P_1^{MP} as a wintertime counterpart of P_2^{MP} is supported. Positive P_2^{MP} corresponds to a weakened Aleutian low, while a reduction of storm activity over the North Pacific is consistent with a shallow mixed layer and the positive SST anomalies of T_1^{P}. Such reasoning should apply primarily in the late winter and early spring (Elsberry and Garwood, 1978), although Niebauer (1980) finds a significant negative correlation between wintertime cloudiness and *annually averaged* SST.

The coupling between the low-level atmospheric circulations over the Arctic and the North Pacific is shown by the $<P^{HP}P^{MP}>$ correlations of Figure 9. The coupling is consistent with the signs of the anomalies within the individual eigenvectors, e.g., positive $<P_1^{HP}P_2^{MP}>$, negative $<P_3^{HP}P_1^{MP}>$, positive $<P_3^{HP}P_2^{MP}>$. However, the coupling is generally weaker than the coupling between North Pacific SLP and SST in terms of both the magnitudes of the largest correlations and the maximum lags of the statistically

significant correlations. The coupling is especially weak during the late spring and early summer. A pertinent feature of the $<P^{HP}P^{MP}>$ diagrams is their general symmetry about 0 lag. There is therefore no apparent tendency for the arctic circulation to drive or be driven by the North Pacific circulation.

Finally, the coupling between the arctic SLP and North Pacific SST fields is shown by the $<P^{HP}T^{P}>$ diagrams of Figure 9. Not surprisingly, this coupling is even weaker than the Arctic/Pacific SLP coupling. The largest correlations are the positive wintertime $<P_2^{HP}T_2^{P}>$, which imply that southward airflow over the Bering Strait is associated with below-normal SSTs over a broad area of the North Pacific from 35°N to 55°N. The correlations of 0.5-0.6 agree well with Niebauer's (1980) correlations for the Pribiloff Island region during 1973-1979. As in the case of the $<P^{HP}P^{MP}>$ correlations, there is no apparent tendency for the arctic SLP fields to lead or lag the SST fields in any systematic manner.

The relationships between summertime ice extent along the northern Alaskan coast (I_{NA}, Figure 2) and the amplitudes of $\underset{\sim}{T}^{P}_{1}$, $\underset{\sim}{P}^{HP}_{2}$, $\underset{\sim}{P}^{HP}_{3}$ and $\underset{\sim}{P}^{MP}_{3}$ are shown in Figure 10a. The amplitudes of the SLP and SST patterns were again smoothed with a 3-month running mean prior to the computations. The correlations are plotted against the calendar month of the midpoint of each 3-month period. Figure 10a contains plots for all those SLP and SST variables that correlate with I_{NA} at a statistically significant (95%) level in at least two consecutive 3-month periods. (The small values of $<I_{NA}P_3^{HP}>$ are plotted only for comparison with $<I_{NA}P_2^{HP}>$). The patterns correlating most highly with I_{NA} are $\underset{\sim}{T}^{P}_{1}$ and $\underset{\sim}{P}^{HP}_{2}$. A relationship between I_{NA} and P_2^{HP} is not surprising, since positive P_2^{HP} describes a flow pattern with a strong

onshore component in the northern Alaskan region. However, the statistical significance of the correlation of I_{NA} with P_2^{HP} of the previous winter and spring was not expected. While I_{NA} correlates most highly with the May-June-July value of P_2^{HP} ($r = 0.61$), I_{NA} correlates significantly with the P_2^{HP} values of every month of the December-July period except February. The results therefore imply that onshore airflow during the previous winter and spring does contribute to the severity of summer ice conditions along the northern Alaskan coast. Later figures will support the interpretation of summer ice extent as an integrated response to atmospheric forcing over the previous 6-12 months. By contrast, the alongshore (east-west) component of the airflow, P_3^{HP}, does not correlate significantly with I_{NA} during any month.

The magnitudes of the correlations between T_1^P and I_{NA} are also unexpectedly large. $\langle I_{NA} T_1^P \rangle$ exceeds even $\langle I_{NA} P_2^{HP} \rangle$ in the 3-month periods centered on every calendar month except January. The high persistence of SST anomalies is evident in the slow decay of $\langle I_{NA} T_1^P \rangle$ after the summer ice season. The positive sign of $\langle I_{NA} T_1^P \rangle$ implies that above-normal ice extent along the northern Alaskan coast ($I_{NA} > 0$) is associated with above-normal SSTs in the 30°N-45°N band of the North Pacific and with below-normal SSTs in the Aleutian region and along the west coast of North America ($T_1^P > 0$). While the mass (water) influx through the Bering Strait is northward into the Chukchi Sea, inflow rates (e.g., Coachman and Aagaard, 1974) appear to be too low to permit a "direct" association between winter/spring Bering Sea SST's and northern Alaskan ice conditions during the following summer. If Bering Strait inflow is a factor in the interannual variability of northern Alaskan ice conditions, current fluctuations and attendant variations in water stress must also be considered. An alternative hypothesis concerning

the relatively large positive values of $\langle I_{NA} T_1^P \rangle$ is that anomalously strong southward airflow (positive P_2^{HP}) prior to heavy ice summers is a factor contributing to both heavy Alaskan ice and to the below-normal SSTs in the Aleutian region. However, this interpretation does not explain the fact that $\langle I_{NA} T_1^P \rangle$ exceeds $\langle I_{NA} P_2^{HP} \rangle$ in nearly every month. The interplay between surface airflow, ocean temperatures and currents, and seasonally varying ice conditions in the Alaskan waters is undoubtedly complex. More detailed and systematic measurements of oceanic parameters are clearly required before the interpretations described above can be regarded as more than the speculative rationalizations of observational data.

Figure 10b shows the correlations between ice extent during February-April in the Bering Sea, I_{BS}, and the amplitudes of $\underset{\sim}{T}_1^P$, $\underset{\sim}{T}_2^P$, $\underset{\sim}{P}_2^{HP}$, $\underset{\sim}{P}_1^{MP}$ and $\underset{\sim}{P}_3^{MP}$. No other SST or SLP fields correlated at 0.5 or higher with I_{BS} in any month. The positive correlations between I_{BS} and the first two SST patterns indicate an association between heavy Bering Sea ice and below-normal SSTs ($T_1^P > 0$, $T_2^P > 0$) in the Aleutian region. While T_2^P correlates significantly with I_{BS} only during and after the late-winter ice maximum, the positive T_1^P of the previous summer and autumn correlate significantly with I_{BS}. A direct association between heavy ice and below-normal SSTs is strongly suggested, especially in view of the relatively narrow time frame (January-April) during which the patterns of southward airflow (P_3^{MP} and P_2^{HP}) correlate significantly with Bering Sea ice. The below-normal SSTs in heavy ice years are evidently not responses to the atmospheric flow patterns that have contributed to the heavy ice. The concentration of significant $\langle I_{BS} P_3^{HP} \rangle$ and $\langle I_{BS} P_2^{HP} \rangle$ into the winter months suggests that Bering Sea ice is a response to a considerably shorter period of atmospheric forcing than is

northern Alaskan ice. The interpretation of the dual peak of $\langle I_{BS} P_1^{MP} \rangle$ is not straightforward. One possible explanation is that positive P_1^{MP}, which was described earlier as a summer mode, is associated with heavy wintertime ice via its strong negative correlation with summer temperatures in the Bering Sea (positive $\langle P_1^{MP} T_1^{P} \rangle$). Persistence of these negative SSTs into winters of heavy Bering Sea ice would then link I_{BS} with positive P_1^{MP} of the preceding summer. This interpretation is supported by the tilt of the $\langle P_1^{MP} T_1^{P} \rangle$ diagram during the summer, autumn and early winter months (Figure 9).

As a final application of the eigenvector representation of the North Pacific data, Figure 11 illustrates the cumulative nature of the atmospheric and oceanic forcing of northern Alaskan and Bering Sea ice. The correlations with ice extent are plotted as functions of the number of months (*prior to* the appropriate ice minimum/maximum) over which the atmospheric and oceanic amplitudes have been averaged. The diagrams therefore show the dependence of the ice indices on the length of the forcing period prior to 31 August in the case of I_{NA} and prior to 31 March in the case of I_{BS}. The correlation between I_{NA} and P_2^{HP}, for example, ranges from 0.19 when based on the single-month August value of P_2^{HP} to 0.84 when based on the mean value of P_2^{HP} for the 9-month period of December-August. The correlation then decreases as the averaging period is increased further, i.e., as months prior to December are included in P_2^{HP}. The results imply that $(0.84)^2 \simeq 0.71$ of the variance of the summertime northern Alaskan ice cover is attributable to variations in a single pattern of airflow over the nine months ending in August. This result is considerably more optimistic than the forecast skills of Walsh and Johnson (1979b, Figure 18), which were based on data from single months and on a more general longitudinal formulation of ice

variability. While the notion of the "usefulness" of correlative results is subjective, application-dependent, and distinct from statistical significance, the explanation of more than 70% of the variance of I_{NA} by one meteorological index, P_2^{HP}, implies considerable potential for long-range ice forecasting in the northern Alaskan region. This potential is supported by the physical plausibility of positive $<I_{NA}P_2^{HP}>$.

Figure 11 also shows that the Bering Sea ice responds to a relatively shorter period of atmospheric forcing (P_2^{HP}, P_3^{MP}) than does the northern Alaskan ice, since the correlations with I_{BS} begin to decay when the averaging period exceeds 3-5 months. Correlations with the SST parameter T_1^P, on the other hand, increase to 0.72 at 5 months for northern Alaskan ice and to 0.56 at 10 months for Bering Sea ice. Persistence of the SST anomalies is again apparent in the weaker dependence of the SST correlations on the length of the averaging period.

In order to show that significant spatial relationships are not obscured by the eigenvector representations, we have plotted in Figure 12 the correlations of the northern Alaskan and Bering Sea ice indices with actual SLP grid point anomalies during the preceding months of significant atmospheric forcing. The correlations were evaluated for all SLP points on a 5°x10° latitude-longitude grid from 20°N poleward. Figure 12a shows that heavy summertime ice conditions are preceded by low pressure to the east and high pressure to the west of the northern Alaskan coast. While I_{NA} correlates more highly with the pressures to the east rather than the west, the highest 7-month correlators are the pressure anomalies in the central North Pacific. A similar pattern was apparent in Rogers' (1978, Figure 2) plot of ice-derived summer pressure differences, although little mention was made of the

Pacific Ocean area in Rogers' work. The pattern in Figure 12a is suggestive of patterns $\underset{\sim}{P}_3^{MP}$ and $\underset{\sim}{P}_2^{HP}$ in the North Pacific and the Arctic, respectively. Interestingly, the highest correlations of Figure 12a are smaller than those derived from the 7-month means of the eigenvector amplitudes. A corresponding correlation map for the 3 months preceding the Bering Sea ice maximum (late March) is shown in Figure 12b. A stronger-than-normal southward component of airflow is indicated. The broad areas of negative correlations over North America and positive correlations over the midlatitude North Atlantic are features that were not captured by the Pacific eigenvectors. However, the magnitudes of the highest correlations are similar to the eigenvector-derived magnitudes in Figure 11b.

Finally, Figure 13 contains maps of the correlations between actual grid point values of SST and the ice indices I_{NA} and I_{BS}. Correlations with North Alaskan ice are weakly negative in the Aleutian region and more strongly negative off the west coast of North America. Since positive correlations are found in the central portion of the grid, the overall correlation pattern is quite similar to $\underset{\sim}{T}_1^P$. The fact that I_{NA} correlates more highly with the amplitude of T_1^P than with the actual SSTs is pertinent to the nature of the I_{NA}/SST association. Since most of the variability within T_1^P is in the broad region of positive anomalies in midlatitudes (Figure 5), positive $\langle I_{NA} T_1^P \rangle$ is indicative primarily of the association between heavy ice and *positive* SST anomalies south of 45°N. This relationship suggests that the I_{NA}/SST coupling is not so much a direct association between heavy ice and low SSTs but rather an indirect association involving the atmosphere (Figure 1). The corresponding map of Bering Sea ice correlations (Figure 13b) contains larger correlations in the Alaskan longitudes. The Bering SST anomalies

associated with heavy ice are negative and are correlated as strongly with I_{BS} as is T_1^P. Again, the overall pattern of grid point correlations shows a resemblance to T_1^P. We conclude that the eigenvector representation has captured the features of the SST fields that are most pertinent to sea ice variability.

b. North Atlantic sector

Since the eigenvectors for the North Atlantic region (Figures 6-8) generally correspond closely with the Pacific patterns (Figures 3-5), the following discussion will emphasize the similarities and differences between the correlative results for the two regions.

Figure 14, which is the Atlantic counterpart of Figure 9, shows the seasonal and lag dependences of the correlations between the amplitudes of the North Atlantic SLP and SST patterns. The diagrams of the midlatitudes SLP/SST correlations show the same characteristic tilt that was found in the Pacific area. SST anomalies can again be interpreted as very persistent responses to forcing by the SLP fields. In the Atlantic diagrams, however, there is very little evidence of SST/SLP associations during the summer months. Since the monthly dependence of the fraction of variance described by $\underset{\sim}{P}_1^{MA}$ does not show a non-winter peak of the type found with the corresponding Pacific pattern $\underset{\sim}{P}_1^{MP}$, there is indeed no justification for the interpretation of $\underset{\sim}{P}_1^{MA}$ as a summer mode. However, the Atlantic diagrams do show that the second and third SST amplitudes, T_2^A and T_3^T, are significantly correlated with P_1^{MA} during the winter half of the year. The positive signs of these correlations suggest that the associations are at least partially attributable to advection by $\underset{\sim}{P}_1^{MA}$ of warm water into the western North Atlantic (T_2^A) and cold water into the waters immediately south of Greenland and Iceland (T_3^A).

Figure 14 also shows that the coupling between the midlatitude and high-latitude SLP fields of the Atlantic region is similar to that in the Pacific sector. Correlations between the P^{MA} and P^{HA} are statistically significant, detectable in all seasons, and generally symmetric about 0 lag. No systematic tendency for either region to lead the other is apparent. Similarly, there are significant correlations between the North Atlantic SST fields and the high-latitude SLP fields. While the $\langle P^{HA} T^{A} \rangle$ diagrams show a tendency toward greater significance at positive lags of T^{A}, there are weak suggestions of a feedback in the opposite direction in $\langle P_1^{HA} T_1^{A} \rangle$ and $\langle P_2^{HA} T_3^{A} \rangle$.

Figure 15a shows the relationships between summertime ice extent in the East Greenland Sea (I_{EG}) and the highest correlators among the (3-month mean) patterns of SST and SLP. The only significant correlations ($r \geq 0.41$) are those with the second, third and fourth high-latitude circulation patterns. While even these correlations are not large, they are consistent with advectional considerations in the sense that southward flow precedes heavy ice. None of the midlatitude SLP or SST fields correlate significantly with I_{EG}, perhaps because the East Greenland Sea is the northernmost of the four ice regions in this study. The closest grid points of SST and midlatitude SLP are approximately 20 latitudinal degrees south of the summertime ice edge in the East Greeland Sea.

The highest correlations with the Denmark Strait ice index, I_{DS}, are shown in Figure 15b. The most striking feature of Figure 15b is the absence of significant correlations. Correlations between I_{DS} and the SLP amplitudes P_1^{MA} and P_1^{HA} are marginally significant (95% level) in only one 3-month period, December-February. The only significant SST correlator is T_3^{A}, which correlates negatively with I_{DS} and most strongly in the months *after* the ice maximum.

As a counterpart of Figure 11, Figure 16 shows the dependence of East Greenland and Denmark Strait ice indices on the length of the period over which the forcing data are averaged. The correlations between I_{EG} and the high-latitude SLP amplitudes, P_2^{HA} and P_4^{HA}, increase out to forcing periods of 5-7 months. $\langle I_{EG} P_2^{HA} \rangle$ remains relatively constant until 11 months. $\langle I_{EG} T_4^A \rangle$ shows a slow but systematic increase through 11 months. Correlations involving the Denmark Strait ice index show little dependence on the forcing interval, although very gradual increases in the magnitudes of $\langle I_{DS} T_3^A \rangle$ and $\langle I_{DS} T_4^A \rangle$ are apparent. $\langle I_{DS} P_2^{HA} \rangle$ is consistently small but positive.

Plots corresponding to Figure 12 were constructed in order to illustrate the relationships between the North Atlantic ice indices and the actual grid point pressures of the previous months. Figure 17a shows the correlations between the East Greenland index and the SLPs for the five months ending in July. A broad area of negative correlations (pressures below normal in heavy ice years) extends from the waters east of the East Greenland Sea to approximately 170°E. The most negative values are near Severnaya Zemlya and the Laptev Sea. This pattern implies not only abnormally strong southward flow in the East Greenland passage but an acceleration of the entire transpolar drift stream from the Chukchi Sea to the Greenland-Spitsbergen passage. An enhanced transpolar drift during the spring and summer would be expected to contribute to heavy summer ice conditions in the East Greenland Sea (Haupt and Kant, 1976). Since Figure 17a shows no high correlations in regions other than the eastern Arctic, East Greenland ice variability is evidently decoupled from midlatitude processes to a greater extent than is Alaskan ice.

Figure 17b supports the eigenvector-based conclusion that ice in the Denmark Strait is associated only weakly with the low-level atmospheric circulation in nearby regions. Marginally significant positive correlations (above-normal pressures in heavy ice years) are found off the southeast coast of Greenland. The only other correlations exceeding 0.4 in magnitude are in the low latitudes, as suggested by the negative $\langle I_{DS} P_1^{MA} \rangle$ of Figure 15.

Correlations between I_{EG}, I_{DS} and the actual grid point values of North Atlantic SST are not shown because of the lack of any substantial areas of statistical significance. The SST grid point correlations therefore support Figure 15 which showed that SST *patterns* do not correlate well with subsequent sea ice in the North Atlantic. The same lack of significance was found when ice/SST correlations were recomputed using monthly North Atlantic SST data compiled by the ICES (International Council for the Exploration of the Sea) Hydrographic Service. Using the ICES data set, Schell (1970) described associations between SST and the *subsequent* atmospheric circulation fields during selected extreme ice years in the North Atlantic. Correlations between Greenland-Barents Sea ice and subsequent SSTs ranged from -0.26 to -0.50 for a set of 49 years. While these correlations are comparable to those obtained here (Figure 15), Schell did not present results for positive lags of sea ice. On the other hand, Rogers and van Loon (1979) found significant correlations between the atmospheric circulation and subsequent ice extent in the Newfoundland region, the Davis Strait and the Baltic Sea. These ice fluctuations were associated with the seesaw of temperature between northwestern Europe and northeastern North America. Unfortunately, our ice regions, the East Greenland Sea and the Denmark Strait, are near the "nodal line" of the seesaw. The results from these previous studies are therefore not inconsistent with the results of the present work, although we

note that our conclusions concerning the absence of significant SST/sea ice associations at positive ice lags may be largely due to our particular choices of sea ice zones.

Finally, the lack of significant SLP/ice as well as SST/ice associations in the Denmark Strait implies either that the ice dynamics in this region are somewhat unique, that I_{DS} is an inappropriate ice index, or that the physical signals have been obscured by erroneous data. While it is possible that I_{DS} is contaminated by some ice data of low quality, the SST consistency tests described in Section 2 suggest that errors in the North Atlantic SST data are more likely to have contributed to a dilution of the SST/ice correlations. Nonetheless, the SST and SLP data show enough consistency with each other (Figure 14) that the small correlations with I_{DS} cannot be attributed solely to errors in the SST and/or SLP data.

5. SUMMARY

This work has been an examination of sea ice fluctuations in the context of the corresponding large-scale ice-ocean-atmosphere systems. Goals were the evaluation of the directions and relative strengths of the various links in the three-component systems, the evaluation of the time scales of the various contributions to interannual ice variability, and a comparison of ice-ocean-atmosphere interactions in the Pacific and Atlantic hemispheres. While the results are limited to the regions we have chosen, the most pertinent conclusions are:

(i) The dominant patterns of SST variability are similar in the North Atlantic and the North Pacific. In both oceans the air-sea coupling is such that the SST anomalies appear as

persistent responses to atmospheric forcing.

(ii) The high-latitude atmospheric circulation is significantly correlated with the circulation fields over both the North Atlantic and the North Pacific. The midlatitude circulations show no systematic tendency to lead or lag the arctic circulation.

(iii) The best predictor of interannual sea ice variability in the four sea ice zones examined here is the north-south component of the high-latitude circulation. Correlations between ice extent and the strength of this component over periods of several months are as large as 0.84 in the marginal ice zone north of Alaska.

(iv) The coupling between the SST distribution and subsequent sea ice extent is stronger in the North Pacific than in the North Atlantic. The correlative analysis suggests a direct associaton between positive (negative) SST anomalies and light (heavy) ice in the Bering Sea. The nature of the SST/ice association north of Alaska is most likely one in which the atmosphere serves as an intermediate link, although such a conclusion is quite tentative in the absence of more detailed information on ocean current variability in the vicinity of the Bering Strait.

(v) The predictability of sea ice appears to be greater in the Alaskan sector than in the two North Atlantic regions examined in this study. Atmospheric forcing over a period of up to 9 months contributes to summer ice variability along the northern Alaskan coast, while atmospheric forcing over 3-4

months is significantly correlated with Bering Sea ice variability.

(vi) Although sea ice fluctuations in the East Greenland Sea appear to be decoupled from SLP and SST fluctuations in middle latitudes, they are significantly correlated with the intensity of the geostrophic airflow parallel to the transpolar drift stream during the previous 5-7 months.

A more definitive analysis of air/sea/ice coupling in high latitudes will clearly require data on the variability of ocean currents in the marginal ice zone. The present analysis may indeed have suffered from the lack of such data for the Bering Strait and the East Greenland region. However, our conclusion that SST/ice associations are detectable form existing data in the North Pacific but not in the North Atlantic underscores the need for a set of systematic measurements of oceanic variables in high latitudes.

ACKNOWLEDGMENTS

This work was sponsored by the Arctic Institute of North America with the approval and financial support of the Office of Naval Research under contract N00014-75-C-0635 (subcontract ONR-463). Computing facility support was provided by the National Center for Atmospheric Research and the University of Illinois Research Board. We wish to thank J. Namias and R. Born for providing the North Pacific temperature data, M. Peterson for assisting with the computations, K. Garrelts for typing the manuscript, and J. Brother for drafting the figures.

REFERENCES

Albright, M., Geostrophic wind calculations for AIDJEX, in Sea Ice Processes and Models (R. Pritchard, Ed.), pp. 402-409, University of Washington Press, Seattle, 1980.

Barnett, D. G., A practical method of long-range ice forecasting for the north coast of Alaska, in Sea Ice Processes and Models (R. Pritchard, Ed.), pp. 360-372, University of Washington Press, Seattle, 1980.

Broccoli, A. J., and R. P. Harnack, Predictability of monthly North Pacific sea level pressure from monthly sea surface temperature using regression models for the period 1933-1976, submitted to J. Geophys. Res., 1981.

Coachman, L. K., and K. Aagaard, Physical oceanography of arctic and subarctic seas, in Marine Geology and Oceanography of the Arctic Seas Y. Herman, Ed.), pp. 1-81, Springer-Verlag, New York, 1974.

Davis, R. E., Predictability of sea surface temperature and sea level pressure anomalies over the North Pacific Ocean, J. Phys. Oceanogr., 6, 249-266, 1976.

Davis, R. E., Predictability of sea level pressure anomalies over the North Pacific Ocean, J. Phys. Oceanogr., 8, 233-246, 1978.

Elsberry, R. L., and R. W. Garwood, Jr., SST anomaly generation in relation to atmospheric storms, Bull. Amer. Meteorological Soc., 59, 786-789, 1978.

Elsberry, R. L., and S. D. Raney, Sea surface temperature response to variations in atmospheric wind forcing, J. Phys. Oceanogr., 8, 881-887, 1978.

Harnack, R. P., and A. J. Broccoli, Associations between sea surface temperature gradient and overlying mid-tropospheric circulation in the North Pacific region, J. Phys. Oceanogr., 9, 1232-1242, 1979.

Haupt, I., and V. Kant, Satellite ice surveillance studies in the Arctic in relationship to the general circulation, in Proceedings of the Symposium on Meteorological Observations from Space: Their Contribution to the First GARP Global Experiment, pp. 179-187, International Council of Scientific Unions, Paris, 1976.

Haworth, C., Some relationships between sea surface temperature anomalies and surface pressure anomalies, Quart. J. Roy. Meteor. Soc., 104, 131-146, 1978.

Herman, G. F., and W. T. Johnson, The sensitivity of the general circulation to arctic sea ice boundaries: A numerical experiment, Mon. Wea. Rev., 106, 1649-1664, 1978.

Jenne, R. L., Data sets for meteorological research, Tech. Note NCAR-TN/IA-111, 194 pp., Nat. Center for Atmos. Res., Boulder, Colo., 1975.

Lamb, H. H., and H. T. Mörth, Arctic ice, atmospheric circulation and world climate, Geogr. J., 144 (part I), 1-22, 1978.

Lemke, P., E. W. Trinkl and K. Hasselmann, Stochastic dynamic analysis of polar sea ice variability, submitted to J. Phys. Oceanogr., 1980.

Namias, J., Synoptic and climatological problems associated with the general circulation of the Arctic, Trans. Amer. Geophys. Union, 39, 40-51, 1958.

Namias, J., Space scales of sea-surface anomalies and their causes, Fishery Bull., 70, 611-617, 1972.

Namias, J., Negative ocean-air feedback systems over the North Pacific in the transition from warm to cold seasons, Mon. Wea. Rev., 104, 1107-1121, 1976.

Namias, J., and R. Born, Temporal coherence in North Pacific sea-surface temperature patterns, J. Geophys. Res., 75, 5952-5955, 1970.

Niebauer, J., Sea ice and temperature variability in the eastern Bering Sea and the relation to atmospheric fluctuations, J. Geophys. Res., 85, 7507-7516, 1980.

Ratcliffe, R. A. S., Recent work on sea surface temperature anomalies related to long-range forecasting, Weather, 28, 106-117, 1973.

Rogers, J. C., Meteorological factors affecting interannual variability of summertime ice extent in the Beaufort Sea, Mon. Wea. Rev., 106, 890-897, 1978.

Rogers, J. C., The North Pacific Oscillation and eigenvectors of northern hemispheric atmospheric circulation during winter, Coop. thesis 56, 177 pp., Nat. Center for Atmos. Res., Boulder, Colo., 1979.

Rogers, J. C., and H. van Loon, The seesaw in winter temperatures between Greenland and northern Europe. Part II: Some oceanic and atmospheric effects in middle and high latitudes, Mon. Wea. Rev., 107, 509-519, 1979.

Rowntree, P. R., Response of the atmosphere to a tropical Atlantic ocean temperature anomaly, Quart. J. Roy. Meteor. Soc., 102, 607-625, 1976.

Schell, I. I., Arctic ice and sea temperature anomalies in the northeastern North Atlantic and their significance for seasonal foreshadowing locally and to the eastward, Mon. Wea. Rev., 98, 833-850, 1970.

Smirnov, V. I., Opposition in ice redistribution in the waters of the foreign Arctic, Meteorologiya i Gidrologiya, No. 3, 73-77, 1980.

Trenberth, K. E., and D. A. Paolino, Jr., The northern hemisphere sea level pressure data set: Trends, errors and discontinuities, Mon. Wea. Rev., 108, 855-872, 1980.

Walsh, J. E., and C. M. Johnson, An analysis of arctic sea ice fluctuations, 1953-1977, J. Phys. Oceanogr., 9, 580-591, 1979a.

Walsh, J. E., and C. M. Johnson, Interannual atmospheric variability and associated fluctuations in arctic sea ice extent, J. Geophys. Res., 84, 6915-6928, 1979b.

Weare, B. C., Empirical orthogonal analysis of Atlantic Ocean sea surface temperatures, Quart. J. Roy. Meteor. Soc., 103, 467-478, 1977.

Zakharov, V. F., and L. A. Strokina, Recent variations in extent of Arctic Ocean ice cover, Meteorologiya i Gidrologiya, No. 7, 35-43, 1978.

Table 1. Correlations between the sea ice indices of the northern Alaskan waters (NA), the Bering Sea (BS), the East Greenland Sea (EG), and the Denmark Strait (DS). Correlations at lag 0 are computed from values for the same calendar year, correlations at lag 1 from values for successive calendar years. Underlined values are statistically significant at 95% level.

Lag 0

	NA	BS	EG	DS
NA	1.00	.25	<u>-.44</u>	-.07
BS		1.00	-.38	-.35
EG			1.00	<u>.57</u>
DS				1.00

Lag 1

		Lagging			
		NA	BS	EG	DS
leading	NA	.03	.38	-.01	-.18
	BS	.03	<u>.50</u>	-.38	<u>-.43</u>
	EG	.08	.14	-.07	.35
	DS	.22	-.22	-.03	<u>.52</u>

Table 2. Summary of major features of eigenvectors

Pattern	Described Variance (%)	Major feature(s) of pattern (positive amplitude)
Sea level pressure		
$\underset{\sim}{P}_1^{MP}$	25.6	Low pressure in Bering Sea, high pressure in midlatitude Pacific
$\underset{\sim}{P}_2^{MP}$	17.8	High pressure south of Aleutians, low pressure in subtropical Pacific
$\underset{\sim}{P}_3^{MP}$	13.0	Low-pressure trough from Aleutians to western North Pacific
$\underset{\sim}{P}_4^{MP}$	9.0	Low-pressure trough from Kamchatka Peninsula to subtropical Pacific
$\underset{\sim}{P}_1^{HP}$	40.6	Pressure deficit in Pacific sector of Arctic
$\underset{\sim}{P}_2^{HP}$	16.8	Southward geostrophic airflow in Pacific sector of Arctic
$\underset{\sim}{P}_3^{HP}$	12.4	Eastward geostrophic airflow in Pacific sector of Arctic
$\underset{\sim}{P}_4^{HP}$	8.8	Cyclonic anomaly center north of Bering Strait
$\underset{\sim}{P}_1^{MA}$	27.0	Low pressure over southern Greenland, high pressure in mid-latitude Atlantic
$\underset{\sim}{P}_2^{MA}$	14.2	High-pressure belt along 50°N, low pressure in subtropical Atlantic
$\underset{\sim}{P}_3^{MA}$	11.0	Low-pressure trough from Newfoundland to western African coast
$\underset{\sim}{P}_4^{MA}$	8.0	Low-pressure trough from eastern U.S. to western Europe

Table 2. (cont.)

$P_{\sim 1}^{HA}$	43.4	Pressure deficit in Atlantic sector of Arctic
$P_{\sim 2}^{HA}$	16.4	Southward geostrophic airflow east of Greenland
$P_{\sim 3}^{HA}$	10.0	Eastward geostrophic airflow north of 65°N
$P_{\sim 4}^{HA}$	8.4	High pressure over Hudson Bay and over Kara Sea
Sea surface temperature		
$T_{\sim 1}^{P}$	15.6	Positive anomaly centered near 35°N, 160°W; negative anomalies off western U.S.
$T_{\sim 2}^{P}$	10.3	Anomalies negative north of 30°N, small elsewhere
$T_{\sim 3}^{P}$	8.8	Anomalies positive in western N. Pacific, negative in eastern N. Pacific
$T_{\sim 4}^{P}$	6.7	Anomalies negative from Aleutians to 25°N, 175°E; positive elsewhere
$T_{\sim 1}^{A}$	15.2	Positive anomaly centered at 45°N, 35°W; negative anomalies to southwest and northeast
$T_{\sim 2}^{A}$	14.1	Anomalies weak and positive off eastern U.S., negative elsewhere
$T_{\sim 3}^{A}$	11.1	Broad belt of positive anomalies south of 45°N
$T_{\sim 4}^{A}$	7.6	Anomalies positive in north-south band along 40°W, negative to east and west

FIGURE LEGENDS

Fig. 1. Schematic representation of coupling mechanisms between sea surface temperature (SST) and sea ice extent.

Fig. 2. Departures from normal ice-covered area (1953-1977) in the northern Alaskan waters (NA), the Bering Sea (BS), the East Greenland Sea (EG) and the Denmark Strait (DS). (See text for longitudes and calendar months corresponding to ice indices.)

Fig. 3. The first four eigenvectors of midlatitude North Pacific sea level pressure. Percentages of variance described by eigenvectors are given in upper left corners of diagrams.

Fig. 4. The first four eigenvectors of high-latitude sea-level pressure in the Pacific sector.

Fig. 5. The first four eigenvectors of North Pacific sea surface temperature. Shaded regions contain negative anomalies when amplitude of eigenvector is positive.

Fig. 6. The first four eigenvectors of midlatitude North Atlantic sea level pressure.

Fig. 7. The first four eigenvectors of high-latitude sea level pressure in the Atlantic sector.

Fig. 8. The first four eigenvectors of North Atlantic sea surface temperature.

Fig. 9. Lagged cross-correlations between amplitudes of dominant eigenvectors of mid-latitude SLP (P^{MP}), high-latitude SLP (P^{HP}) and sea-surface temperature (T^{P}) in the North Pacific. Calendar months are identified by J = January, F = February, ..., D = December. Contour interval is 0.2; solid contours indicate positive

correlations, dashed contours negative correlations. Magnitudes of correlations exceed 0.4 in shaded regions.

Fig. 10. Cross-correlations between North Pacific sea ice indices and amplitudes of eigenvectors of SLP and SST. Months are identified by J = January, F = February, etc. Dashed lines are 95% significance levels.

Fig. 11. Cross-correlation between North Pacific sea ice indices and amplitudes of SLP and SST averaged over 1, ..., 12 months prior to approximate minimum (northern Alaska) or maximum (Bering Sea) ice extent.

Fig. 12. Cross-correlations between (a) I_{NA} and grid-point SLPs during 7 months ending 31 August, (b) I_{BS} and grid-point SLPs during 3 months ending 31 March. Contour interval is 0.1. Contours between -0.4 and +0.4 are plotted (dashed lines) only in region near North Pacific ice boundary. H and L indicate maxima and minima in correlation fields.

Fig. 13. Cross-correlations between (a) I_{NA} and grid point values of North Pacific SST during 5 months ending in August, (b) I_{BS} and grid point values of North Pacific SST during 5 months ending in March. Contour interval is 0.2; regions of negative correlations are shaded. "+" and "-" indicate maxima and minima in correlation fields.

Fig. 14. As in Fig. 9, but for the North Atlantic.

Fig. 15. Cross-correlations between North Atlantic sea ice indices and amplitudes of eigenvectors of SLP and SST. Months are identified by J = January, F = February, etc. Dashed lines are 95% significance levels.

Fig. 16. Cross-correlations between North Atlantic sea ice indices and amplitudes of SLP and SST averaged over 1, ..., 12 months prior to approximate minimum (East Greenland) or maximum (Denmark Strait) ice extent.

Fig. 17. Cross-correlations between (a) I_{EG} and grid-point SLPs during 5 months ending 31 July, (b) I_{DS} and grid-point SLPs during 5 months ending March 31. Contour interval is 0.1. Contours between -0.4 and +0.4 are plotted (dashed lines) only in regions near North Atlantic ice boundary. H and L indicate maxima and minima in correlation fields.

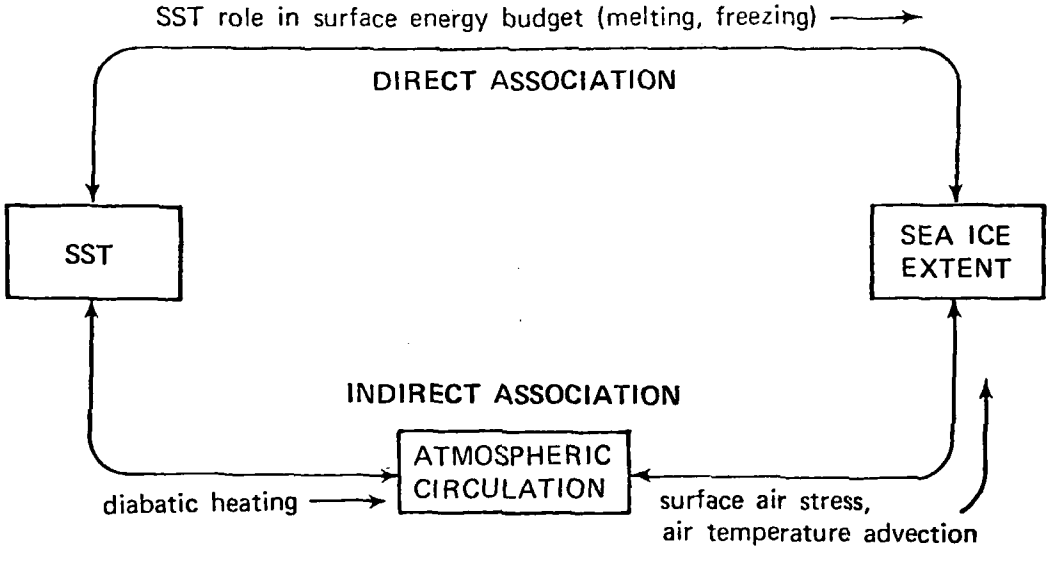

Fig. 1. Schematic representation of coupling mechanisms between sea surface temperature (SST) and sea ice extent.

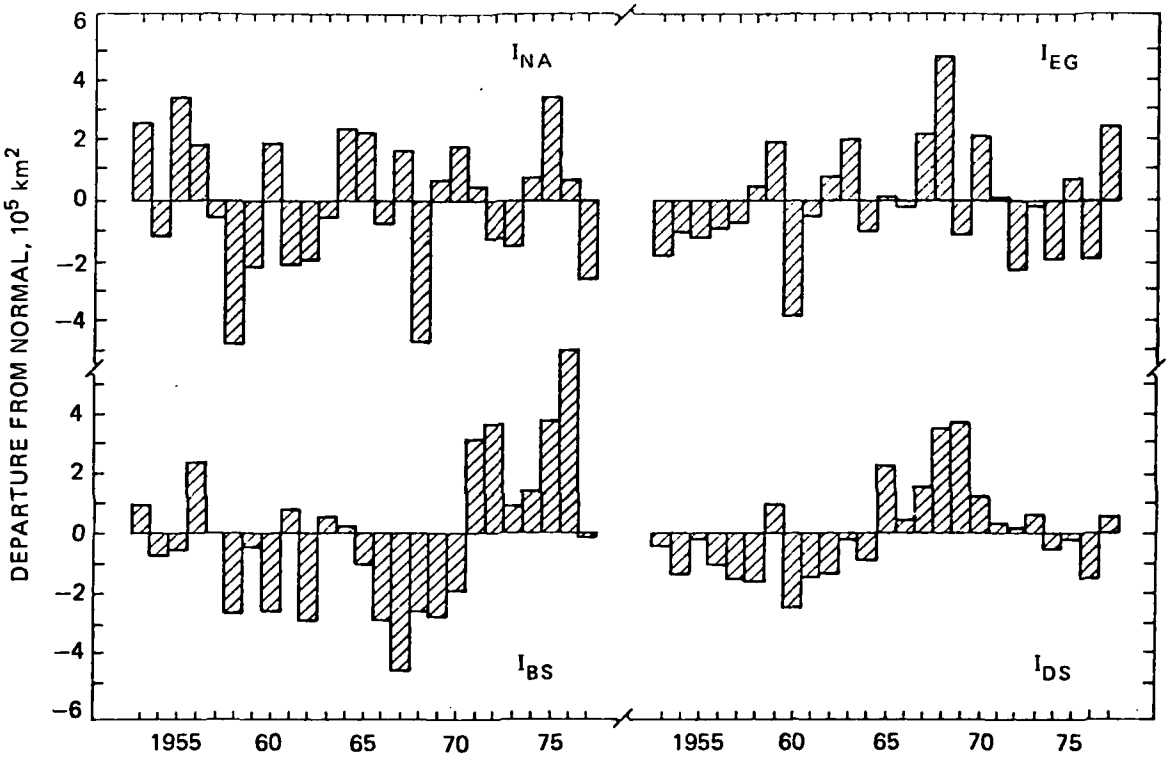

Fig. 2. Departures from normal ice-covered area (1953-1977) in the northern Alaskan waters (NA), the Bering Sea (BS), the East Greenland Sea (EG) and the Denmark Strait (DS). (See text for longitudes and calendar months corresponding to ice indices).

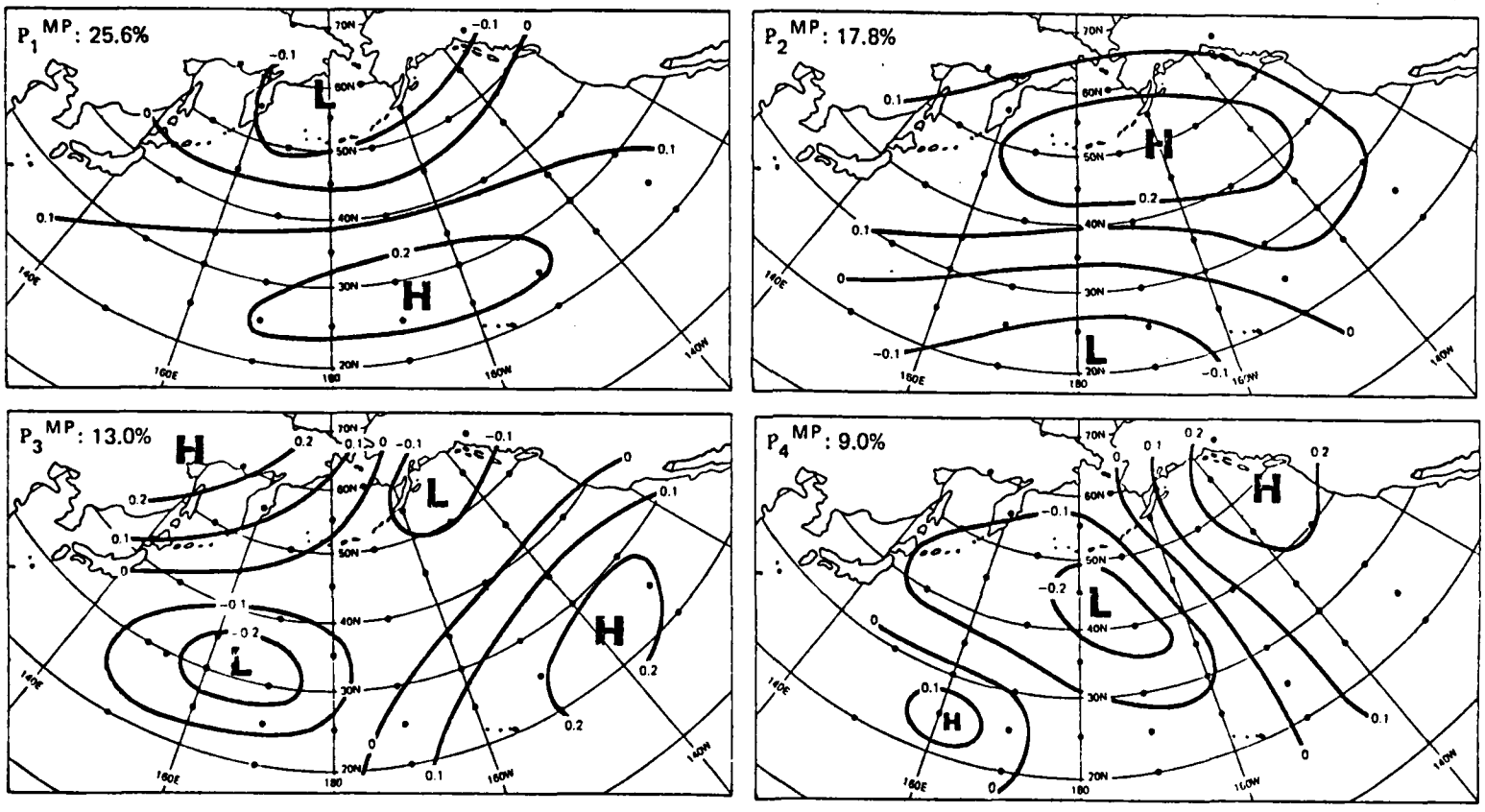

Fig. 3. The first four eigenvectors of midlatitude North Pacific sea level pressure. Percentages of variance described by eigenvectors are given in upper left corners of diagrams.

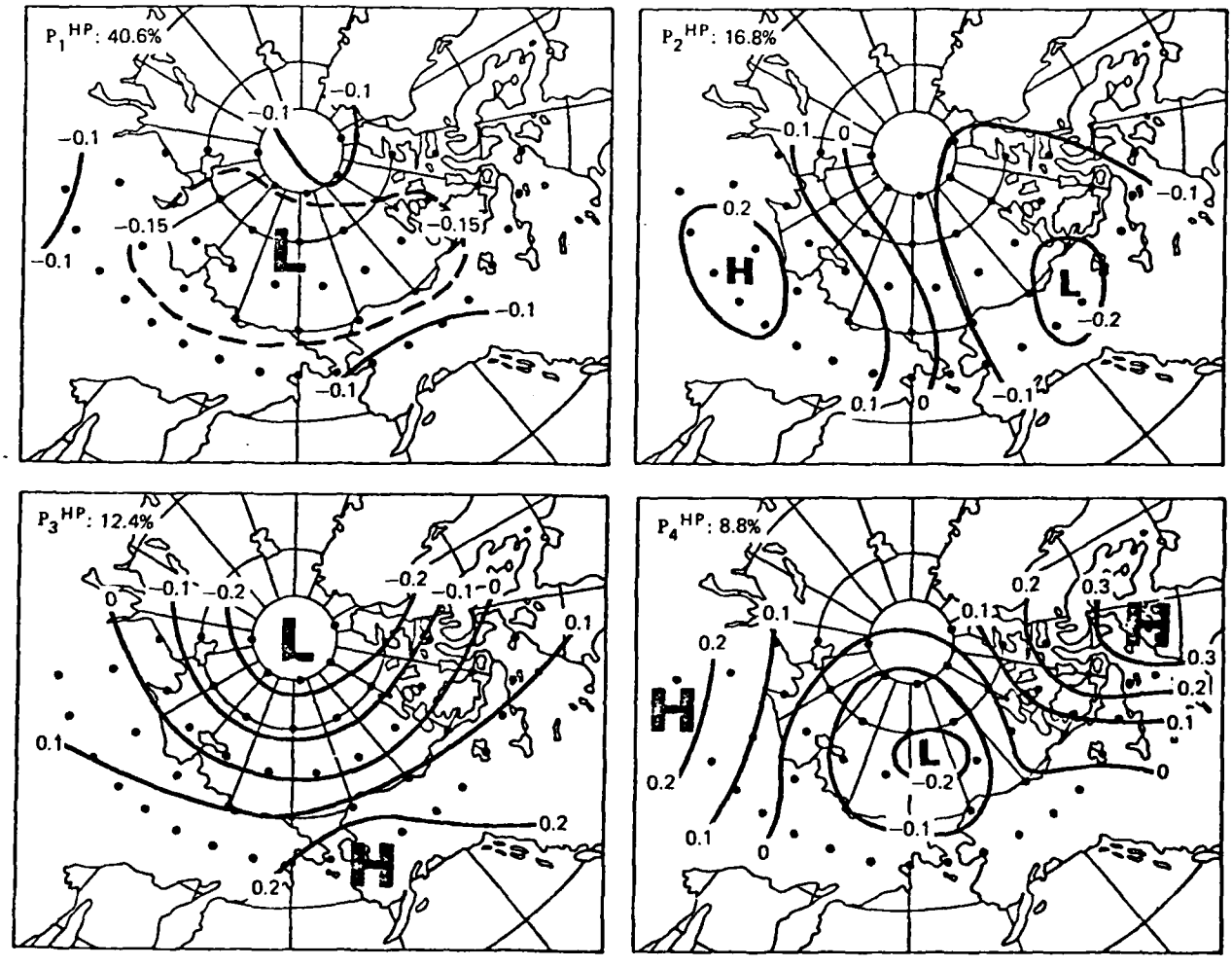

Fig. 4. The first four eigenvectors of high-latitude sea-level pressure in the Pacific sector.

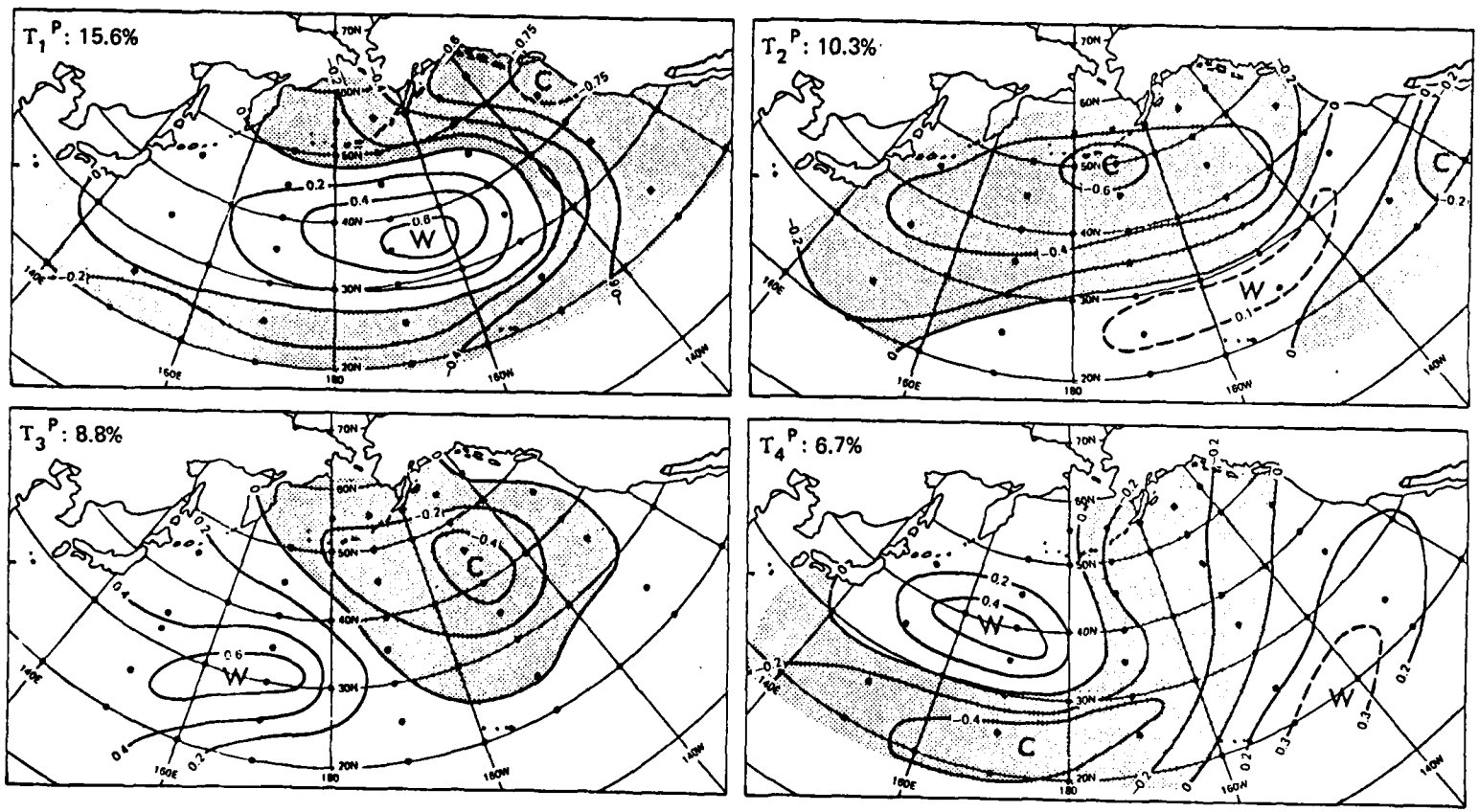

Fig. 5. The first four eigenvectors of North Pacific sea surface temperature. Shaded regions contain negative anomalies when amplitude of eigenvector is positive.

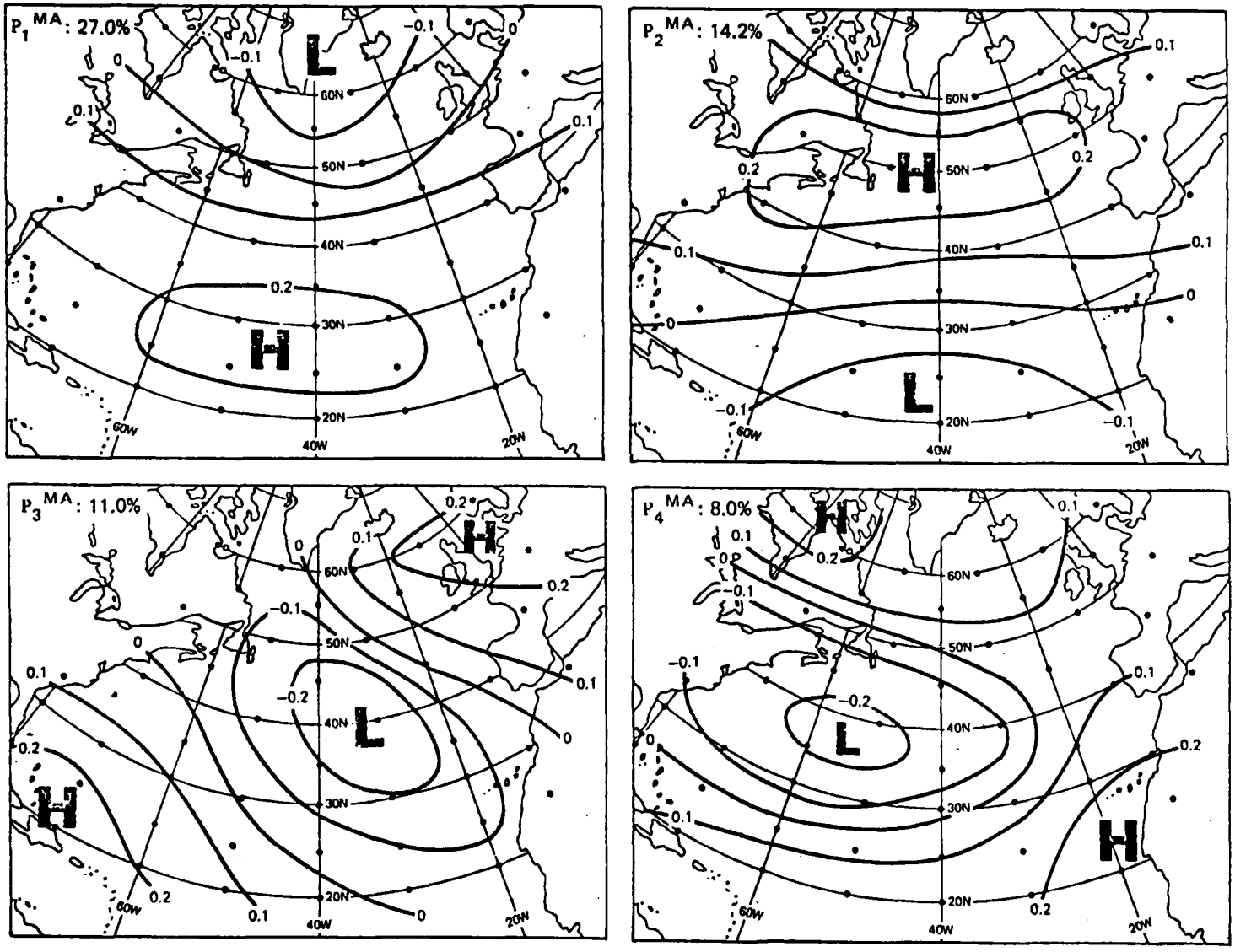

Fig. 6. The first four eigenvectors of midlatitude North Atlantic sea level pressure.

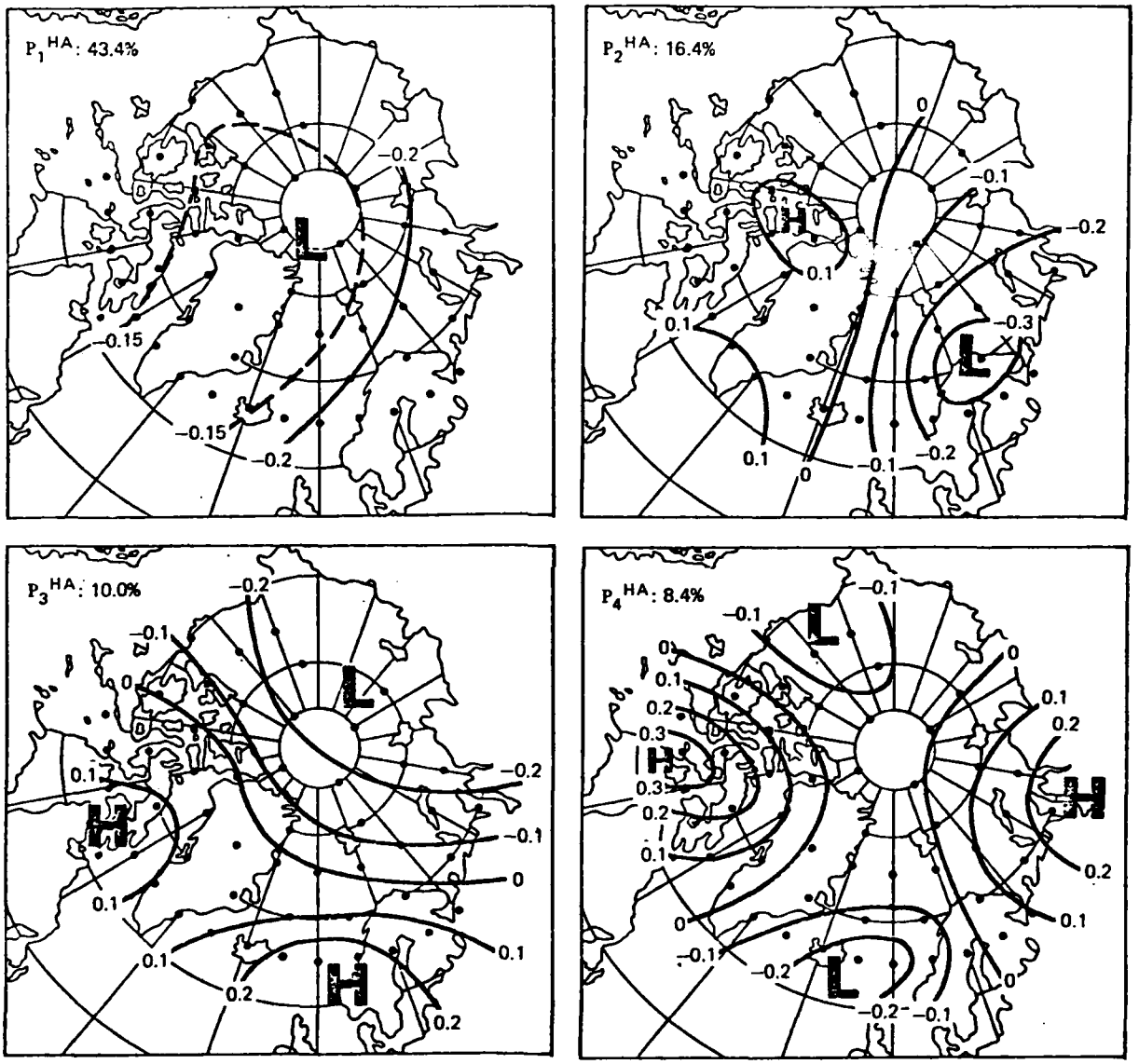

Fig. 7. The first four eigenvectors of high-latitude sea level pressure in the Atlantic sector.

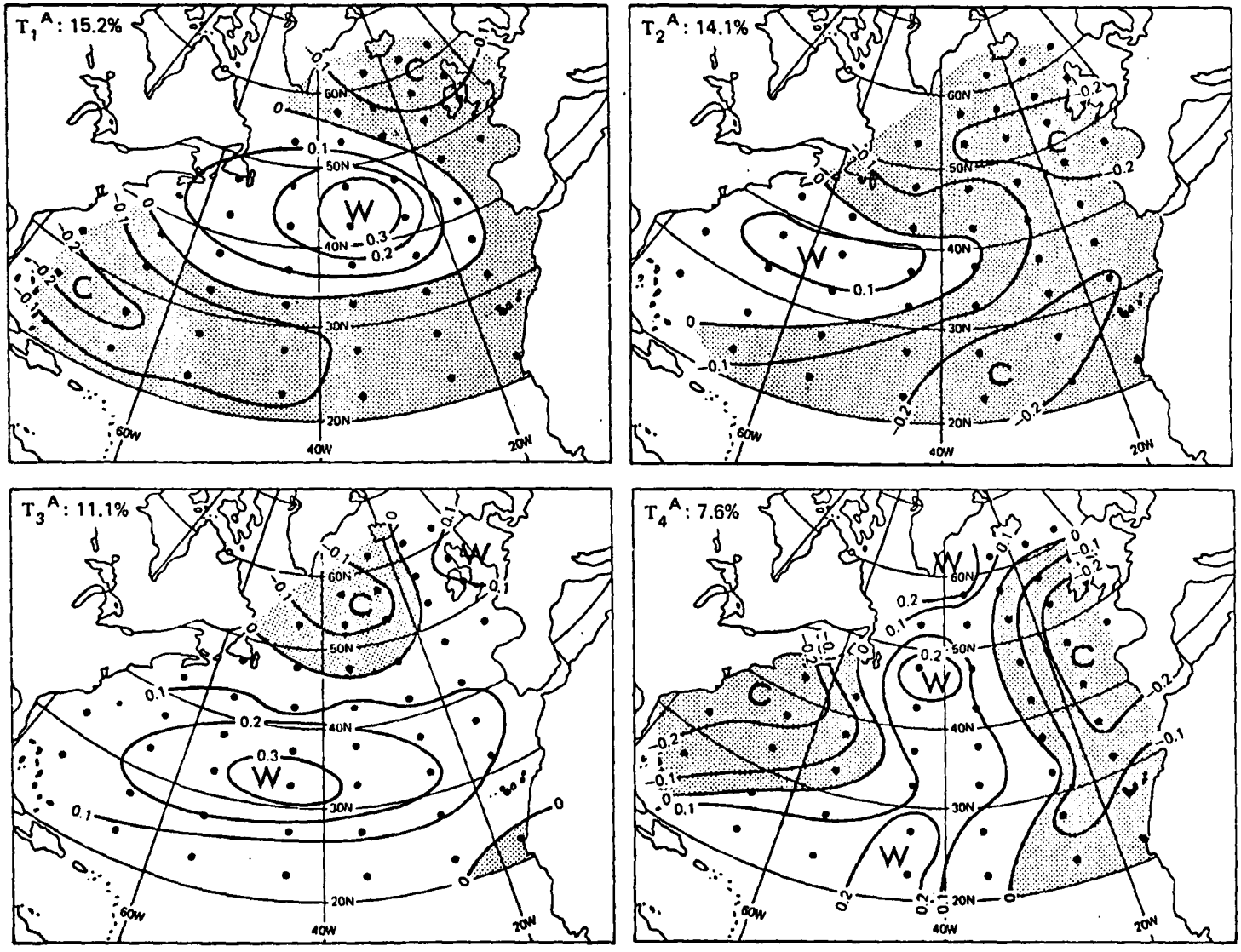

Fig. 8. The first four eigenvectors of North Atlantic sea surface temperature.

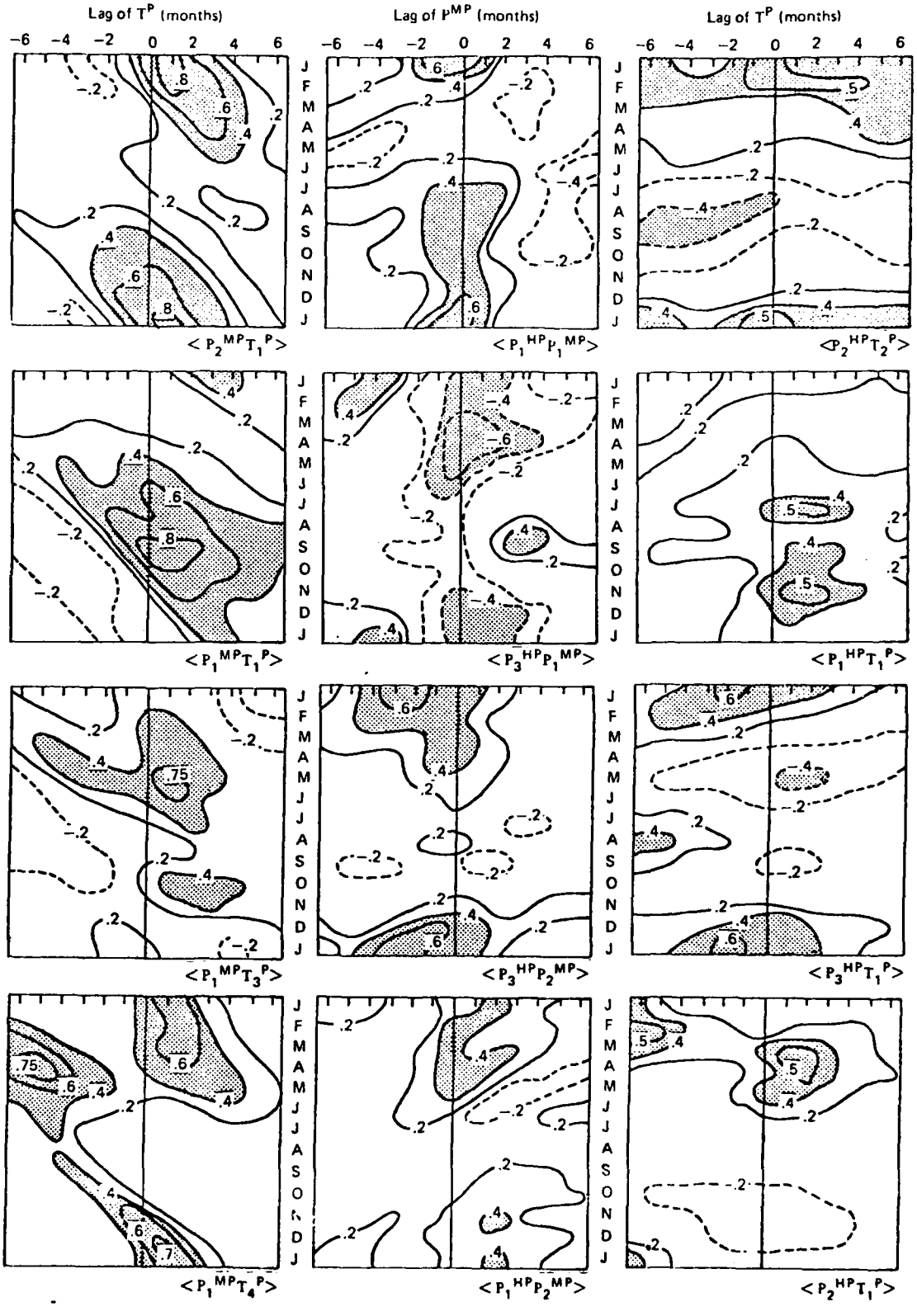

Fig. 9. Lagged cross-correlations between amplitudes of dominant eigenvectors of mid-latitude SLP (P^{MP}), high-latitude SLP (P^{HP}) and sea-surface temperature (T^P) in the North Pacific. Calendar months are identified by J = January, F = February, ..., D = December.

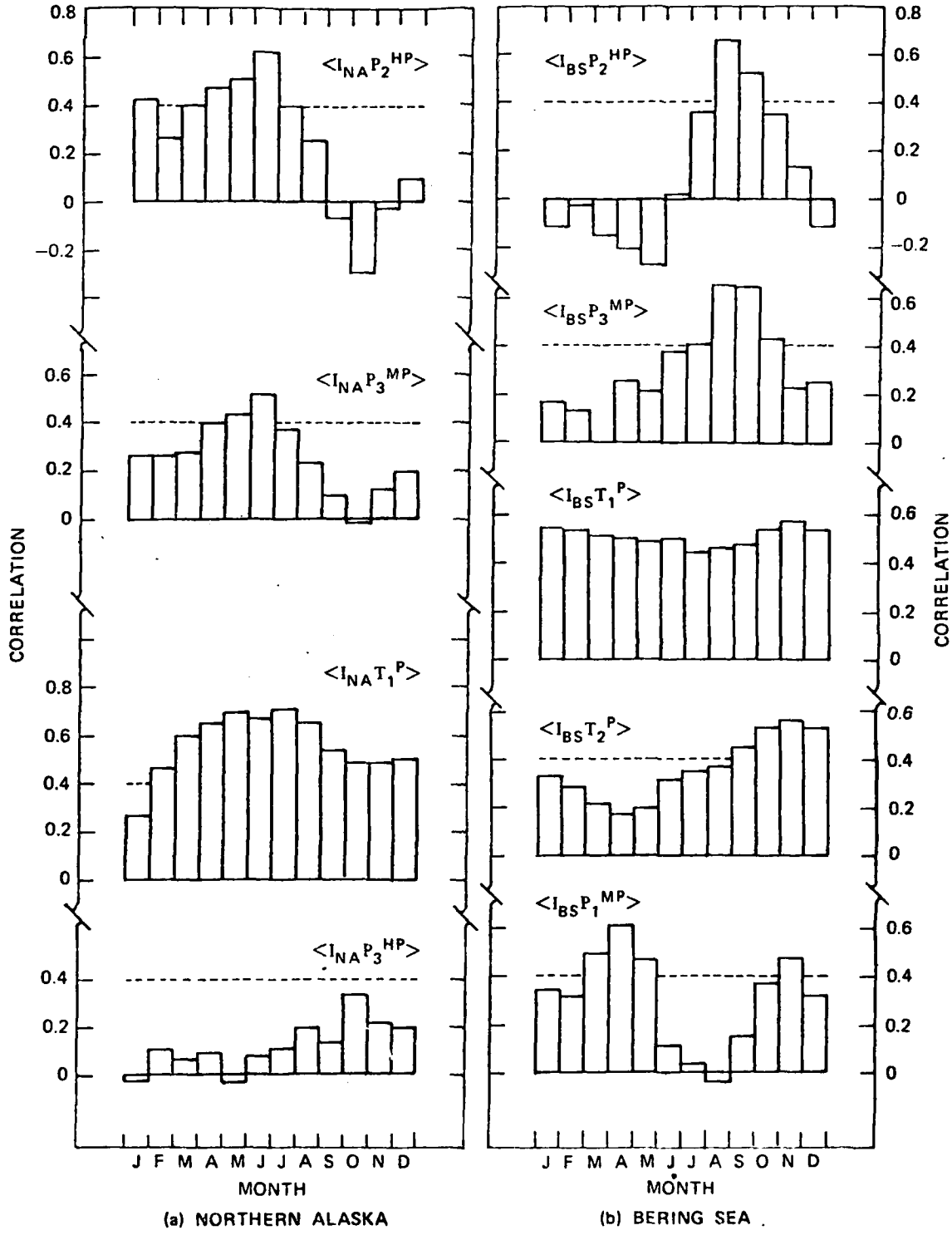

Fig. 10. Cross-correlations between North Pacific sea ice indices and amplitudes of eigenvectors of SLP and SST. Months are identified by J = January, F = February, etc. Dashed lines are 95% significance levels.

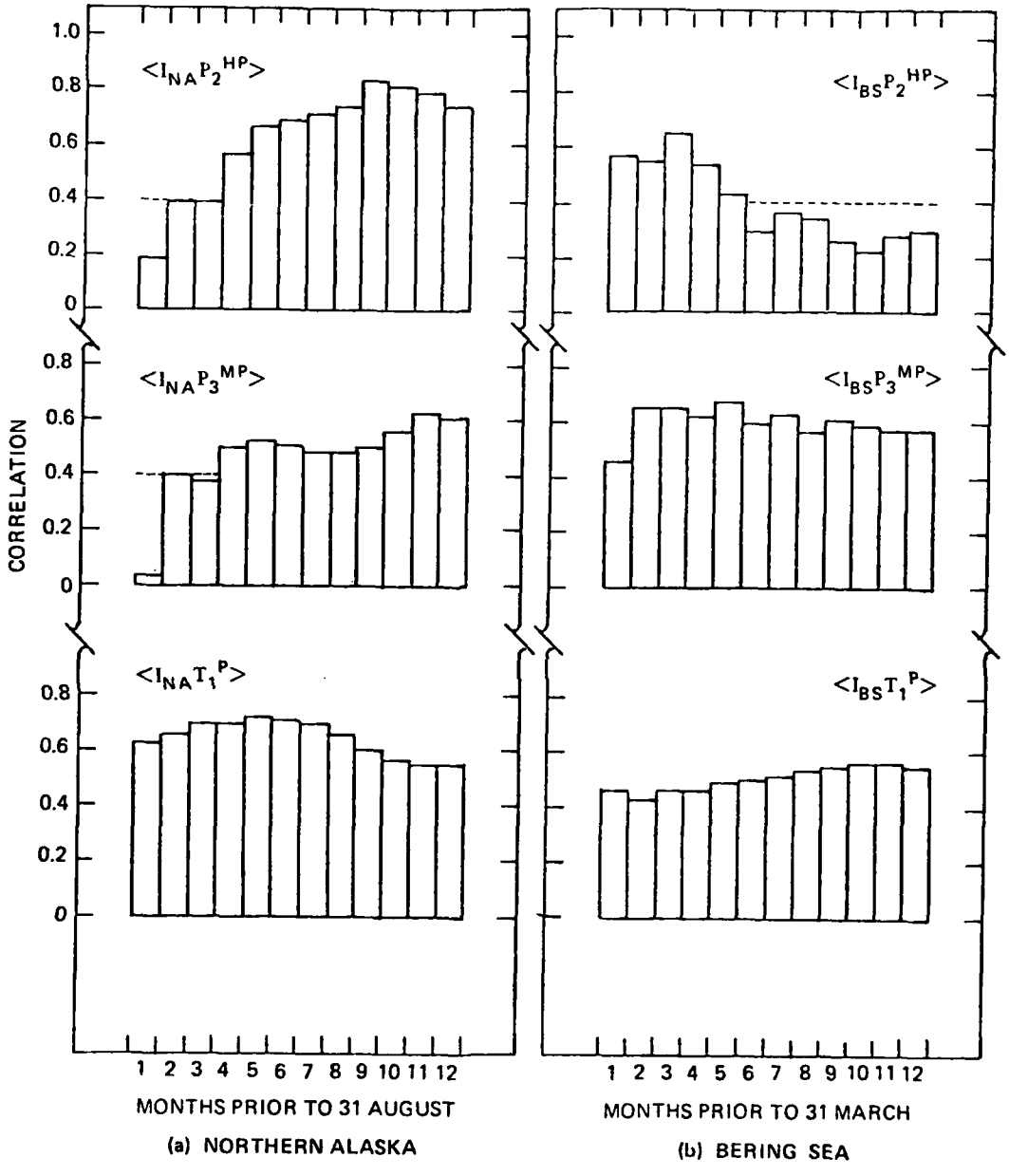

Fig. 11. Cross-correlation between North Pacific sea ice indices and amplitudes of SLP and SST averaged over 1, ..., 12 months prior to approximate minimum (northern Alaska) or maximum (Bering Sea) ice extent.

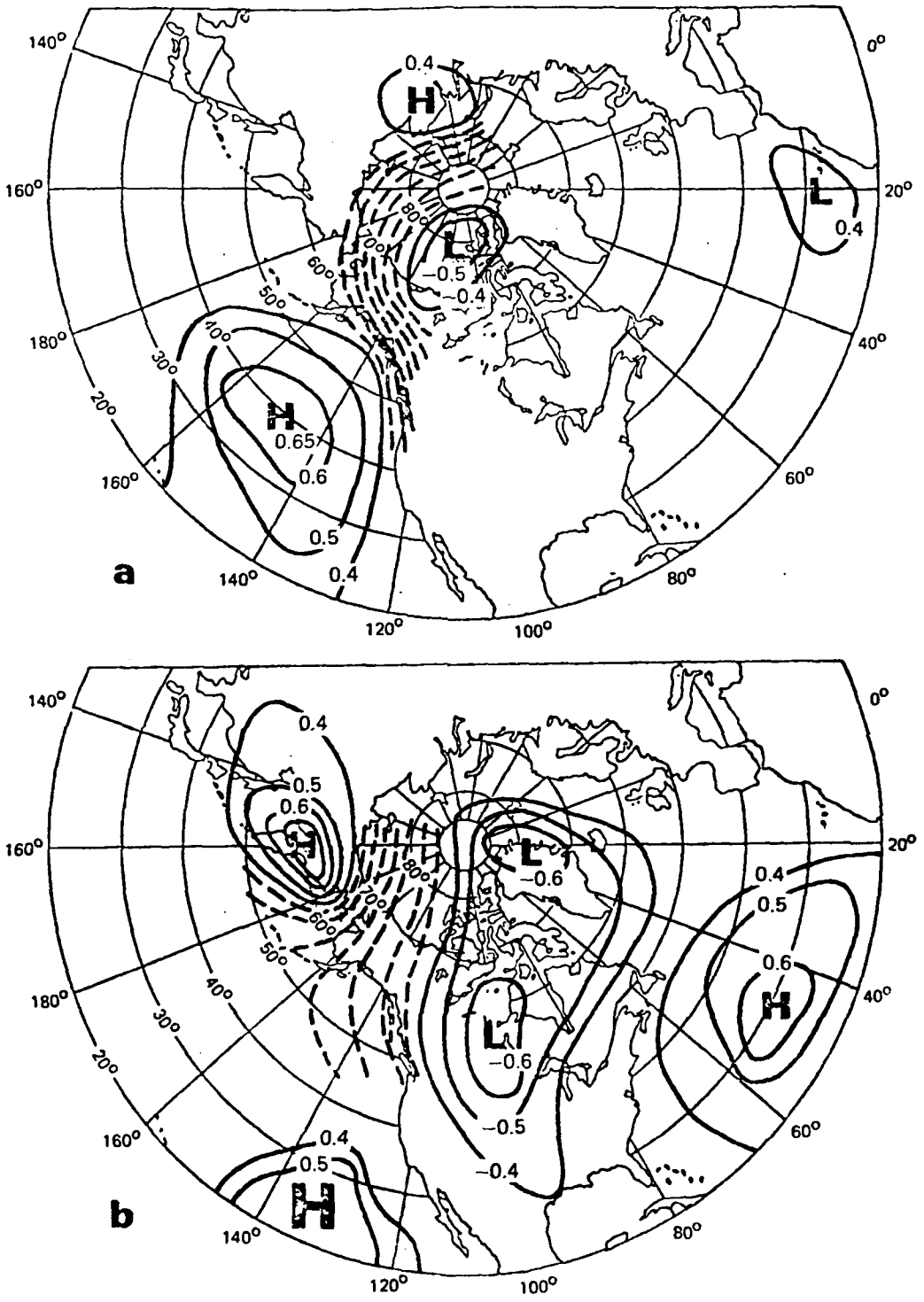

Fig. 12. Cross-correlations between (a) I_{NA} and grid-point SLPs during 7 months ending 31 August, (b) I_{BS} and grid-point SLPs during 3 months ending 31 March. Contour interval is 0.1. Contours between -0.4 and +0.4 are plotted (dashed lines) only in region near North Pacific ice boundary. H and L indicate maxima and minima in correlation fields.

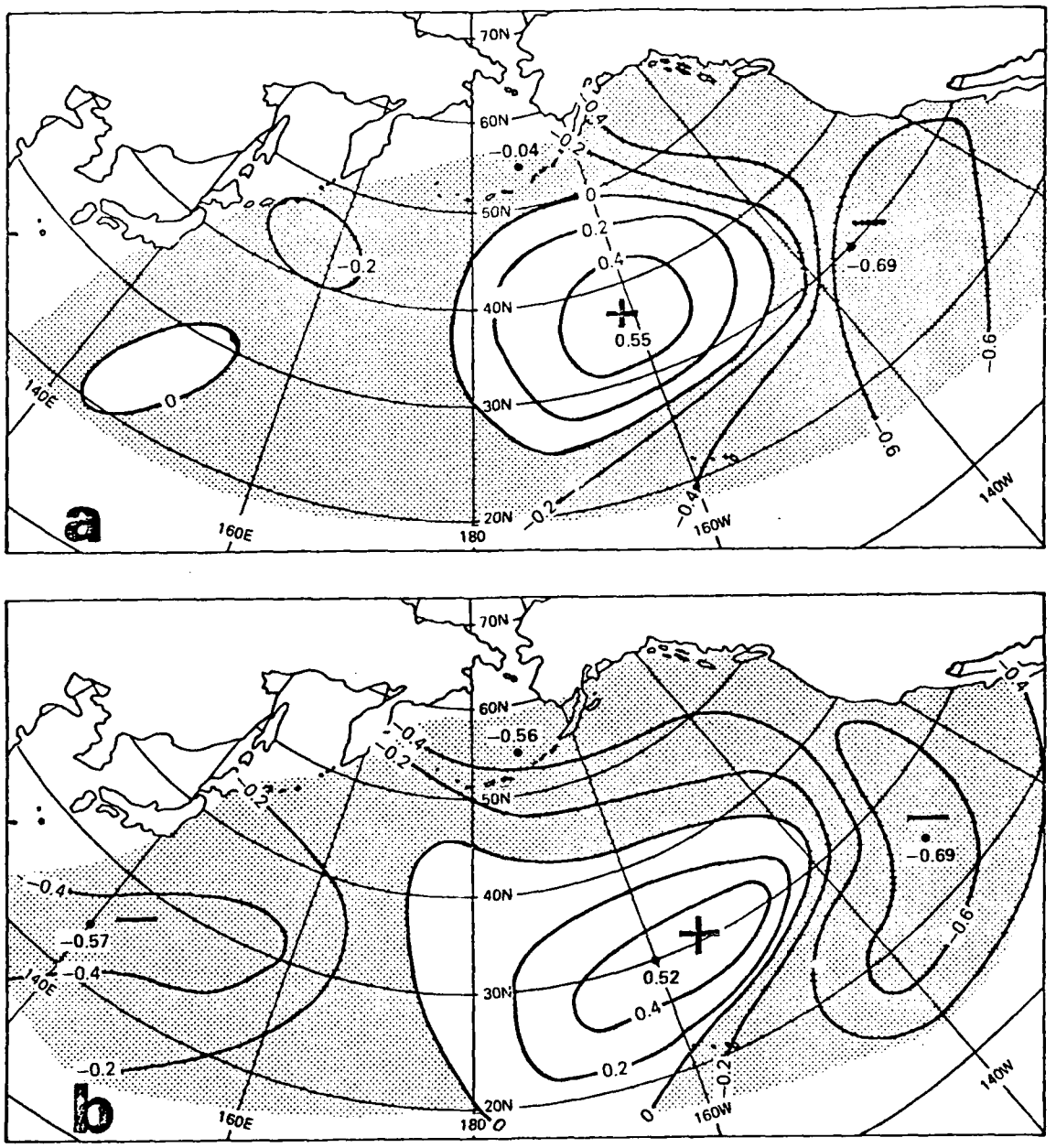

Fig. 13. Cross-correlations between (a) I_{NA} and grid point values of North Pacific SST during 5 months ending in August, (b) I_{BS} and grid point values of North Pacific SST during 5 months ending in March. Contour interval is 0.2; regions of negative correlations are shaded. "+" and "-" indicate maxima and minima in correlation fields.

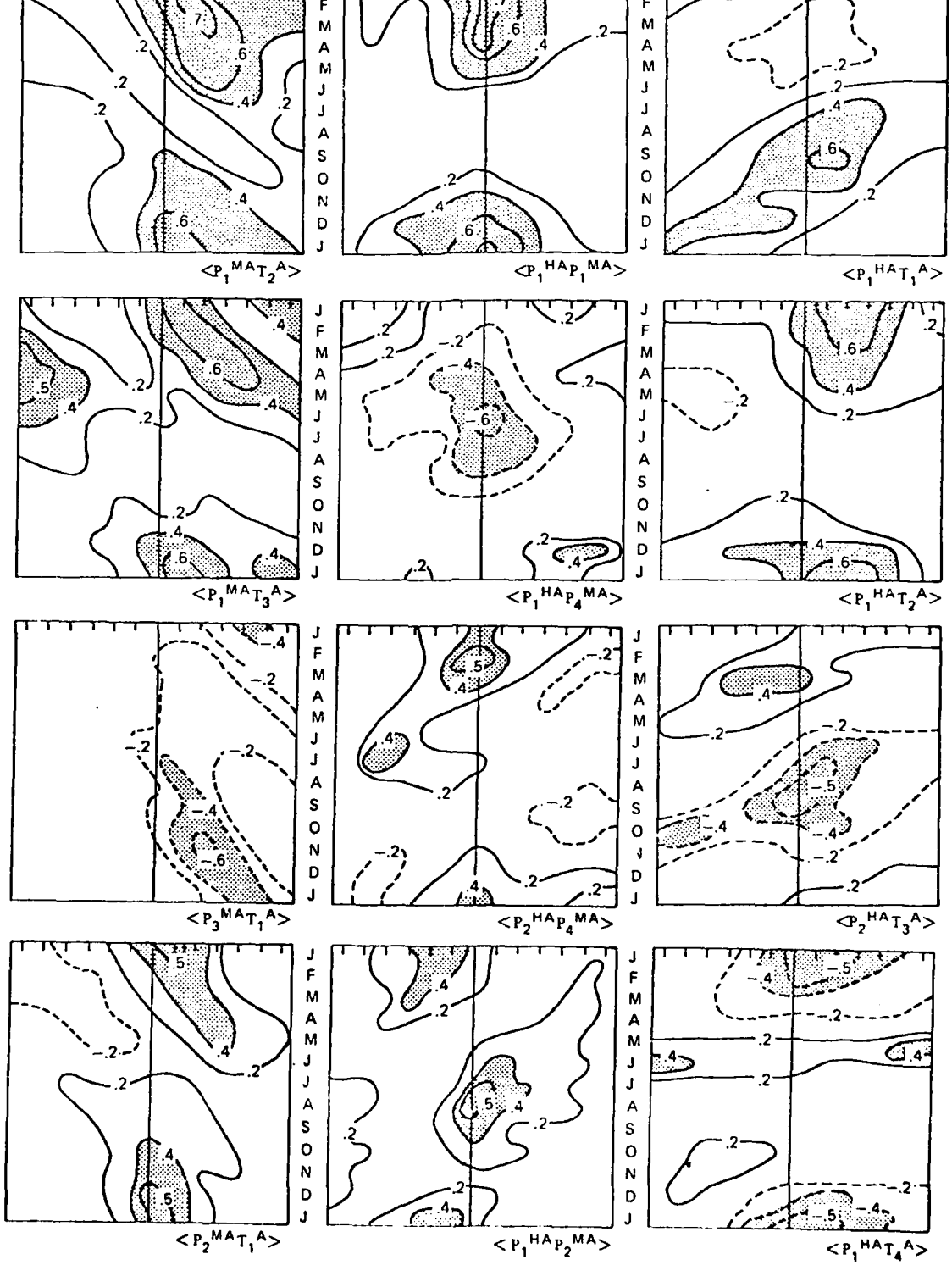

Fig. 14. As in Fig. 9, but for the North Atlantic.

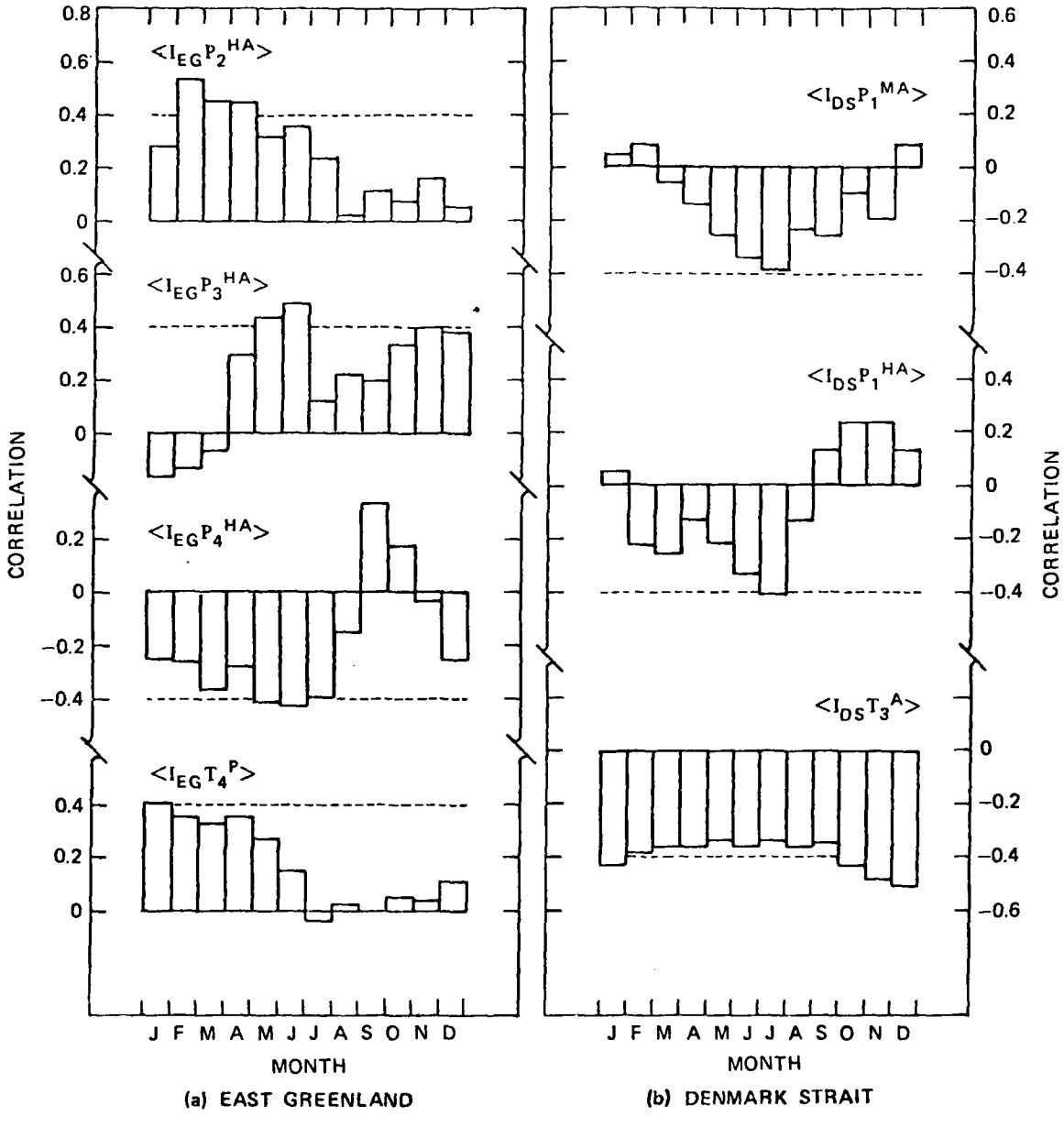

Fig. 15. Cross-correlations between North Atlantic sea ice indices and amplitudes of eigenvectors of SLP and SST. Months are identified by J = January, F = February, etc. Dashed lines are 95% significance levels.

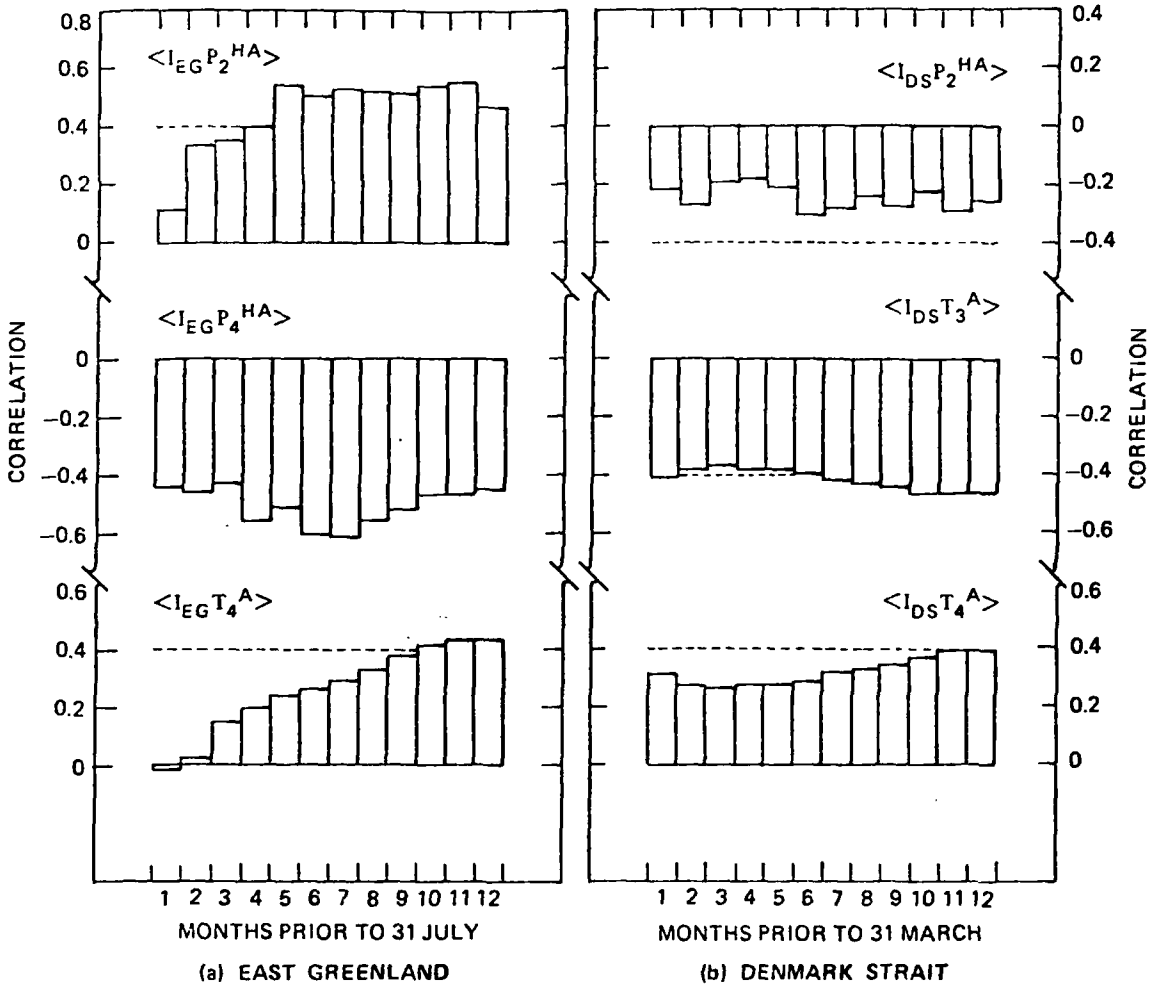

Fig. 16. Cross-correlations between North Atlantic sea ice indices and amplitudes of SLP and SST averaged over 1, ..., 12 months prior to approximate minimum (East Greenland) or maximum (Denmark Strait) ice extent.

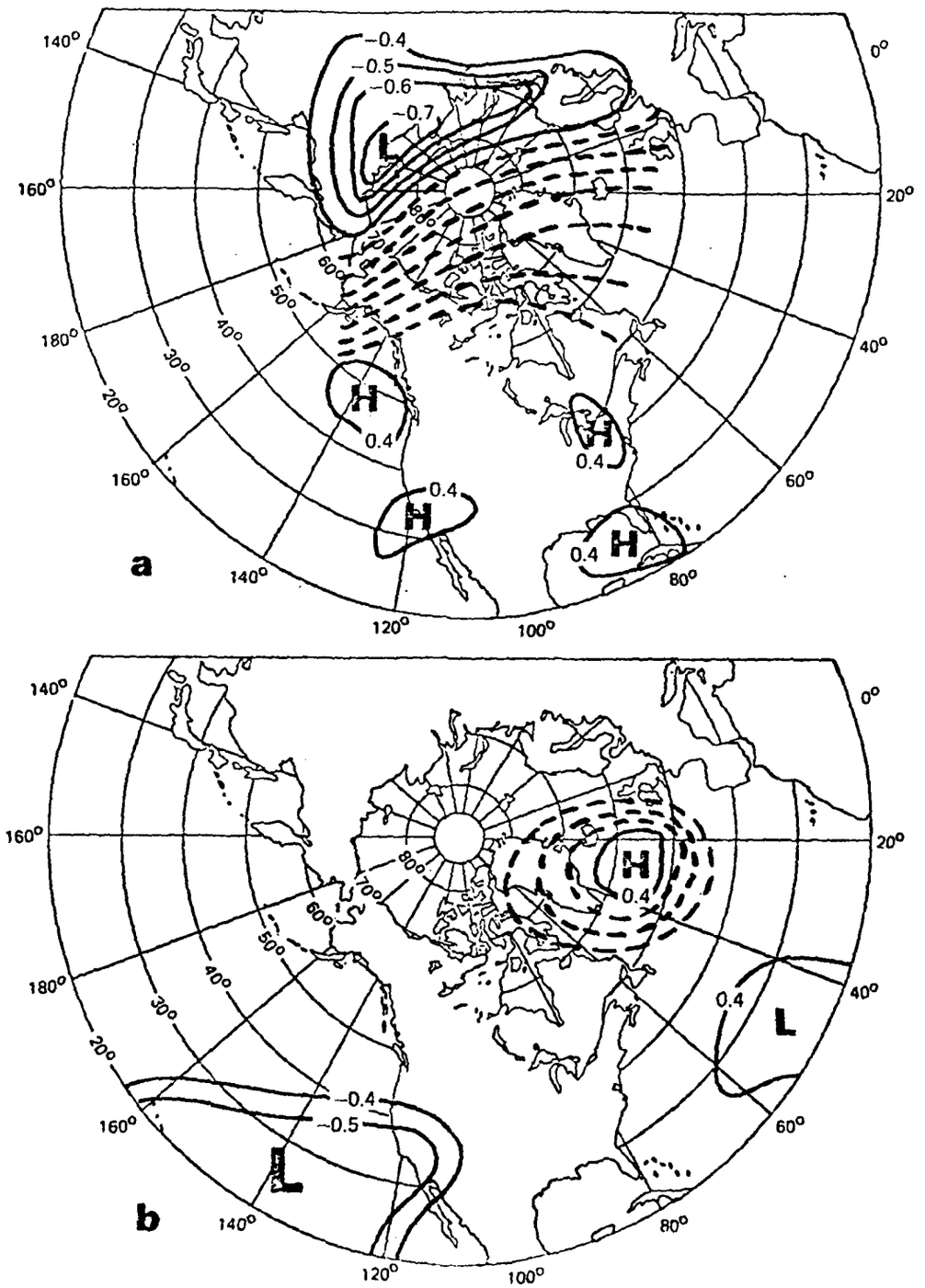

Fig. 17. Cross-correlations between (a) I_{EG} and grid-point SLPs during 5 months ending 31 July, (b) I_{DS} and grid-point SLPs during 5 months ending 31 March. Contour interval is 0.1. Contours between -0.4 and +0.4 are plotted (dashed lines) only in regions near North Atlantic ice boundary. H and L indicate maxima and minima in correlation fields.


N
DATE
ILME